

BAT X-ray Survey - III: X-ray Spectra and Statistical Properties.

M. Ajello¹, A. Rau², J. Greiner¹, G. Kanbach¹, M. Salvato², A. W. Strong¹, S. D. Barthelmy³, N. Gehrels³, C. B. Markwardt³ and J. Tueller³

majello@mpe.mpg.de

ABSTRACT

In this concluding part of the series of three papers dedicated to the *Swift*/BAT hard X-ray survey (BXS), we focus on the X-ray spectral analysis and statistical properties of the source sample. Using a dedicated method to extract time-averaged spectra of BAT sources we show that Galactic sources have, generally, softer spectra than extragalactic objects and that Seyfert 2 galaxies are harder than Seyfert 1s. The averaged spectrum of all Seyfert galaxies is consistent with a power-law with photon index of 2.00 ± 0.07 . The cumulative flux-number relation for the extragalactic sources in the 14-170 keV band is best described by a power-law with a slope $\alpha = 1.55 \pm 0.20$ and a normalization of $9.6 \pm 1.9 \times 10^{-3}$ AGN deg^{-2} (or 396 ± 80 AGN all-sky) above a flux level of $2 \times 10^{-11} \text{erg cm}^{-2} \text{s}^{-1}$ (~ 0.85 mCrab). The integration of the cumulative flux per unit area indicates that BAT resolves 1-2% of the X-ray background emission in the 14-170 keV band. A sub-sample of 24 extragalactic sources above the 4.5σ detection limit is used to study the statistical properties of AGN. This sample comprises local Seyfert galaxies ($z=0.026$, median value) and $\sim 10\%$ blazars. We find that 55% of the Seyfert galaxies are absorbed by column densities of $N_H > 10^{22}$ H-atoms cm^{-2} , but that none is a bona fide Compton-thick. This study shows the capabilities of BAT to probe the hard X-ray sky to the mCrab level.

Subject headings: galaxies: active – surveys – X-rays: binaries – X-rays: galaxies

¹Max-Planck Institut für Extraterrestrische Physik, Postfach 1312, 85741, Garching, Germany

²Caltech Optical Observatories, MS 105-24, California, Institute of Technology, Pasadena, CA 91125, USA

³Astroparticle Physics Laboratory, Mail Code 661, NASA Goddard SpaceFlightCenter, Greenbelt, MD 20771, USA

1. Introduction

There is a general consensus that the cosmic X-ray background (CXB), discovered more than 40 years ago (Giacconi et al. 1962), is produced by integrated emission of Active Galactic Nuclei (AGN). Population synthesis models have successfully shown, in the context of the AGN unified theory (Antonucci 1993), that AGN with various level of obscuration and at different redshifts account for 80–100% of the CXB below 4 keV (Comastri et al. 1995; Gilli et al. 2001; Treister & Urry 2005). Notwithstanding all the advances in the field a major question remains, do Compton-thick sources exist in the numbers that seem to be required by population synthesis models (e.g. Comastri et al. 1995; Gilli et al. 2001) to reproduce the shape of the CXB emission? Indication of the existence of such population comes from the analysis of the CXB fraction which is resolved-into-sources; Worsley et al. (2005) find that such fraction decreases with energy and that the unresolved component is consistent as being the emission of a yet undetected population of Compton-thick AGN. In synthesis, much evidence points towards the existence of Compton-thick AGN while only a handful of them are known and studied.

The >10 keV energy range is the most appropriate band for studying and selecting an unbiased (with respect to absorption) sample of AGN. This band is also the optimum band for the detection of Compton-thick objects. These elusive objects could have been missed because of the difficulties of performing sensitive imaging of the hard X-ray sky. The Burst Alert Telescope (BAT) (Barthelmy et al. 2005), on board the Swift mission (Gehrels et al. 2004) represents a major improvements in sensitivity for X-ray imaging of the hard X-ray sky. We refer to Ajello et al. (2007) for details about the BXS survey.

We applied an innovative image reconstruction algorithm to 8 months of survey BAT data; our survey covers ~ 7000 deg² reaching a limiting sensitivity of < 0.9 mCrab. This makes it one of the most sensitive survey ever performed in the hard X-ray domain. We detected 49 hard X-ray sources of which 37 were previously unknown as hard X-ray emitters. Correlation with X-ray catalogs allowed us to identify 15 sources, while *Swift*/XRT pointed observations provided identification for another 15 objects. Furthermore, we optically identified three new extragalactic sources (Rau et al. 2007). Here, we investigate the spectral and statistical properties of all complete source sample.

The paper is organized as follows. In section 2 we present the X-ray spectral analysis of the BAT sources. The details of the dedicated spectral extraction method are presented in the Appendix A.4. We use the source spectra to build an X-ray color-color plot which is used to understand the mean properties of the source populations. In section 3, we apply the V/V_{MAX} method to test the completeness of the extragalactic sample which is then used

to derive the number-flux relation. The section ends with a discussion about the statistical properties of the extragalactic sample. Finally, we discuss the BAT results in section 4. Throughout this work we use $H_0 = 70 \text{ km s}^{-1} \text{ Mpc}^{-1}$ ($h_{70} = 1$), $k = 0$, $\Omega_{matter} = 0.3$ and $\Lambda_0 = 0.7$ and the luminosities are given in $\text{erg s}^{-1} \text{ h}^{-1}$.

2. Spectral analysis

We have developed a dedicated spectral extraction method which allows to derive the time-averaged spectrum of all sources. The reader interested in the method is referred to the Appendix A for details. Using this method, we derived for all our source candidates a 6 channels energy spectrum in the 14-195 keV. The energy channels used in this analysis are (in keV): 14–22, 22–30, 30–47, 47–71, 71–121, 121–195. The energy bins were optimally chosen to produce similar error bars (in the different energy bins) for sources with power-law spectra.

We found that 21 sources had at least soft X-ray observations by *Swift*/XRT or ASCA. For these sources, we jointly fit XRT/ASCA and BAT data. When fitting a source spectrum, we have preferred the simplest model yielding a good description of the data. The normalization of the ASCA spectra was allowed to vary (with respect to the BAT ones) to cope with the different epochs of the observations. This was not required when fitting XRT and BAT data. In general, the BAT spectrum of Galactic sources is well fitted by a thermal bremsstrahlung model. Instead, AGN are usually better described by a single power-law model. However, when $< 10 \text{ keV}$ data were available the fit required additional components (i.e. black body component for soft excess and/or gaussian model for the iron line). The detailed analysis is reported in Appendix A.4 while the spectral parameters are summarized in Table 1.

The properties of the source sample can be studied using hardness ratios. We have, thus, defined HR_1 and HR_2 as:

$$HR_1 = \frac{\textit{medium} - \textit{hard}}{\textit{medium} + \textit{hard}}, \quad HR_2 = \frac{\textit{soft} - \textit{medium}}{\textit{soft} + \textit{medium}}, \quad (1)$$

where the *soft*, *medium* and *hard* bands are respectively (in keV): 14–30, 30–71, 71–195. The hardness ratios, shown in Fig.1, are normalized to the range -1 and +1. Different symbols indicate different source classes. We also indicate the loci occupied by sources with a power law index in the range 1.0-3.5, or a bremsstrahlung spectrum with a temperature of 5–50 keV. A few things can be derived by the study of the hardness ratios. Galactic sources, which are usually characterized by soft X-ray spectra, have HR_2 values < -0.3 and $HR_1 < -0.5$ which is the typical region for sources with steep photon index. Indeed,

the five Cataclysmic Variables (CVs) present in the sample are all well fit by a relativistic bremsstrahlung model with a mean plasma temperature of 23 keV.

Similarly we note that Sy2 galaxies seem to have (given the large uncertainties) harder X-ray spectra than Sy1s (larger values of HR_1). The fact that type-2 AGN have systematically harder spectra than type-1 could be an evidence of the intrinsic difference between these two classes of objects. In order to study this in more detail we performed a stacked spectral analysis¹ grouping the Seyfert galaxies detected by BAT into three classes: Seyfert 1, Seyfert 2 and intermediate Seyferts. The results, which are summarized in Table 2, show that the mean photon index of Seyfert-1 and Seyfert-2 are different at more than 2σ level. The same trend was previously noted in Seyfert galaxies detected by *OSSE* (Zdziarski et al. 2000) and by *INTEGRAL* (Beckmann et al. 2006). Zdziarski et al. (2000) find that the difference in spectral index could be due to the different viewing angle between Seyfert 1s and 2s. Indeed, the strength of Compton reflection decreases with the increasing viewing angle. Since the spectrum from Compton reflection peaks at 30 keV followed by a steep decline, the larger the reflection component, the softer the spectrum. We tested this scenario using for Seyfert 1s (Seyfert 2s are successfully fitted by a simple power-law) the PEXRAV (Magdziarz & Zdziarski 1995) model in XSPEC. Indeed we get a good fit ($\chi^2 = 1.2/3$) with a (minimum) reflection strength $R > 1.1$ (upper limit is unconstrained by the fit) which is in good agreement with what found by Zdziarski et al. (2000) and Deluit & Courvoisier (2003). Thus, the BAT data seem to confirm the larger reflection component present in Seyfert 1 galaxies (with respect to Seyfert 2s) in agreement with the AGN unified model. Even though, the reflection component improves the fit, it does not affect the photon index of Seyfert 1s which remains 2.30 ± 0.12 .

We note, however, that most of the Seyfert 1s (6 out of 9) have a low value of HR_1 denoting a steep spectrum. We thus tried to fit the stacked spectrum with a cutoff power-law model of the form $E^{-\Gamma} e^{-(E/E_c)}$. Since the power-law index and the e-folding energy E_c are highly correlated we fixed the photon index to 2.0 (see below). The best fit e-folding energy is $110.8_{-33.0}^{+68.4}$ keV (90% C.L.) with a reduced chi-squared which is substantially better than the one of the power-law model (0.9 vs. 1.4 and F-test probability of 0.08). The presence of a cutoff at ~ 100 keV in the X-ray spectra of Seyfert 1 seems also to be confirmed by the analysis of Deluit & Courvoisier (2003).

Finally, we performed the stacked spectral analysis of all the Seyferts to investigate the averaged spectrum of the local AGN detected by BAT. The stacked spectrum, shown in Fig. 2, is consistent (in the 15–200 keV range) with a power-law model of photon index of

¹All stacked spectral analysis are performed doing a weighted average of the spectra.

2.00±0.07 (90% C.L.).

3. The hard X-ray extragalactic sample

The extragalactic sample, shown in Table 3, was derived from the catalog reported in Table 2 of Ajello et al. (2007) considering only objects at $|b| > 15^\circ$ and not spatially associated with the Large Magellanic Cloud. Here we describe the main properties of the sample.

3.1. Completeness of the sample

In order to compute the AGN number-flux relation it is necessary to have a complete and unbiased sample. Since different regions of the sky have different exposure times, we applied in Ajello et al. (2007) a significance limit rather than a flux limit to define our sample. Now we want to test our extragalactic sample for completeness (i.e. derive the significance limit which ensures to include all objects above a given flux limit) and we use the V/V_{MAX} method (Schmidt 1968)². This method which is applied to samples complete to a well-defined significance limit, can also be used to test the completeness level of a sample as a function of significance. For a significance limit below the true completeness level limit of the sample, the V/V_{MAX} returns a value less than $\langle V/V_{\text{MAX}} \rangle_{\text{true}}$ which would be the true test result for a complete sample. Above the completeness limit the $\langle V/V_{\text{MAX}} \rangle$ values should be distributed around $\langle V/V_{\text{MAX}} \rangle_{\text{true}}$ within the statistical uncertainties.

V/V_{MAX} is computed for each source as $(F/(\sigma_{\text{test}}\delta F))^{-3/2}$, where F is the flux, δF is the 1σ statistical uncertainty, σ_{test} is the significance level tested for completeness (and thus the term $\sigma_{\text{test}}\delta F$ is the limiting flux of the sky region where we detected the source), and the exponent $-3/2$ comes from the assumption of no evolution and uniform distribution in the local universe. $\langle V/V_{\text{MAX}} \rangle$ is computed as an average of all sources detected with $S/N \geq \sigma_{\text{test}}$. For a given mean value $m = \langle V/V_{\text{MAX}} \rangle$ and n sources, the error on $\langle V/V_{\text{MAX}} \rangle$ can be computed as (Avni & Bahcall 1980):

$$\sigma_m(n) = \sqrt{\frac{1/3 - m - m^2}{n}} \quad (2)$$

² In this test V stands for the volume where the object has been detected and V_{MAX} is the accessible volume in which the object, due to the flux limit of the survey, could have been found. In case of no evolution $\langle V/V_{\text{MAX}} \rangle = 0.5$ is expected.

The results of the test are shown in Fig. 3. We find a constant value for significances $> 4.5\sigma$. The deviation from the expected 0.5 value is insignificant being less than 1σ .³

We also remark that for completeness we are referring to the threshold above which all sources above the corresponding flux limit are included in the sample. Furthermore, given the small redshift of the sample (see section 3.3) the hypothesis of no evolution is justified.

3.2. Extragalactic source counts

The cumulative source number density can be computed as:

$$N(> S) = \sum_{i=1}^{N_S} \frac{1}{\Omega_i} \quad [\text{deg}^{-2}] \quad (3)$$

where N_S is the total number of detected sources in the field with fluxes greater than S and Ω_i is the sky coverage associated to the flux of the i^{th} source (shown in Fig. 9 of Ajello et al. (2007)).

The cumulative distribution is reported in Fig. 4. We performed a maximum likelihood fit to the cumulative counts assuming a simple power-law model of the form $N(> S) = AS^{-\alpha}$. Here, A is the normalization at $2 \times 10^{-11} \text{ erg cm}^{-2} \text{ s}^{-1}$ and α is the slope. As conventional we used the maximum likelihood estimator (e.g. Crawford et al. 1970) to determine the best fit values. The normalization is not a parameter of the fit, but is obtained assuming that the number of expected sources from the best fit model is equal to the total observed number. The Poissonian error on the total number of sources provides a reliable estimate of its error.

In the 14–170 keV band the best fit parameter is: $\alpha = 1.55 \pm 0.20$ (with normalization $9.6 \pm 1.9 \times 10^{-3} \text{ deg}^{-2}$). The source count distribution is thus consistent with a pure Euclidean function ($\alpha = 3/2$). From our data we expect that the number of all-sky AGN is 396 ± 80 brighter than $2 \times 10^{-11} \text{ erg cm}^{-2} \text{ s}^{-1}$. This corresponds to an integrated flux of $\sim 5 \times 10^{-12} \text{ erg cm}^{-2} \text{ s}^{-1} \text{ deg}^{-2}$ or $\sim 1.5\%$ of the intensity of the X-ray background in the 14–170 keV energy band as measured by HEAO-1 (Gruber et al. 1999).

³It is not uncommon for coded mask detectors to produce a test value slightly above 0.5 (e.g. Beckmann et al. 2006). This is likely caused by systematic errors which tend to increase the $\langle V/V_{\text{MAX}} \rangle$ value.

We can compare the surface density of extragalactic objects found by BAT with previous measurements by converting the BAT fluxes to other energy bands assuming a power law spectrum with photon index of 2.0 (see Section 2) and evaluating the surface density above $10^{-11} \text{erg cm}^{-2} \text{s}^{-1}$.

The results of such comparisons are shown in Tab.4. The BAT surface density is in agreement with the reported measurements, except for the case of the 0.5–2 and 2–10 keV surveys. Indeed, such surveys, at limiting fluxes of $10^{-11} \text{erg cm}^{-2} \text{s}^{-1}$, are biased against the detection of absorbed sources⁴. It is also worth noting that the recent XMM measurement of the 5–10 keV source counts distribution (Cappelluti et al. 2007) is in perfect agreement with our estimate.

3.3. Statistical properties

Above the 4.5σ the extragalactic sample, shown in Table 3, contains 24 AGN. 19 objects are classified as Seyfert galaxies, 3 as blazars, 1 as X-ray bright Optically Normal Galaxy (XBONG) and 1 as Quasar. The identification completeness of such sample is thus 100%.

Excluding the blazars, the median redshift of the sample is $z=0.026$ (mean is $z=0.046$) giving a median luminosity of $10^{43.5} \text{erg s}^{-1}$ (mean is $10^{43.8} \text{erg s}^{-1}$) in the 14-170 keV band. Assuming a hydrogen column density of $10^{22} \text{atoms cm}^{-2}$ as the threshold between absorbed and unabsorbed objects, we find that intrinsic absorption is present in $\sim 55\%$ of the sample. This fraction is lower than the 75% expected by the standard unified model, which is derived by the opening angle of ionizations cones (e.g. Evans et al. 1991). However, this unexpectedly low fraction of absorbed AGN in the local Universe does not seem to pose any particular problem for the understanding and the synthesis of the CXB (e.g. Sazonov et al. 2007).

In Fig. 5 we show the intrinsic column density of the sources as a function of unabsorbed luminosity in the BAT band. Excluding the lower limits on the absorption, we do not find evidences of an anticorrelation between luminosity and absorption. We also note the presence of a rare very luminous ($L_x \sim 10^{45} \text{erg cm}^{-2}$) highly absorbed ($N_H \sim 10^{23} \text{atoms cm}^{-2}$) type-2 QSO. If the lower limits on the absorption will be confirmed, the total fraction of such objects might be in the range 5-15%.

None of the source in Tab. 3, having 2–10 keV measurement, is a Compton-thick AGN. Our claim is supported by several evidences:

⁴The bias decreases in deep fields and thus at lower fluxes (and higher redshifts) because the photoelectric cut-off is redshifted at lower energies.

- As shown by Matt et al. (1997), for the case of NGC 1068, the spectra of Compton-thick AGN might be reflection-dominated (i.e. the reflection component is larger than the transmitted one). We thus tried to fit to each source a pure reflection model (PEXRAV in Xspec). For all the sources, except Mrk 704, the fit is statistically unacceptable. However, Mrk 704 is not a Compton-thick source as Landi et al. (2007) have recently shown.
- Compton-thick sources generally show iron lines with equivalent widths of ~ 1 keV (e.g. Guainazzi et al. 2005). The spectral analysis (see also values in Tab. 3) shows that all sources have iron line equivalent widths smaller than 1 keV.
- The thickness parameter T , defined as $L_{2-10\text{ keV}} / L_{\text{OIII}}$ (see also Bassani et al. 1999), can be used to identify Compton-thick sources (characterized by $T \leq 1$). We computed the thickness parameter for all sources having OIII flux measurements (Rau et al. 2007) and 2–10 keV observations (see Tab. 3). All sources except NGC 2992 (which is however unabsorbed) have thickness parameter values consistent with the values expected for Compton-thin AGN.

We evaluated the radio-loudness of AGN using the R-index defined in Laor (2000) as $R \equiv f_{\nu}(5\text{ GHz}) / f_{\nu}(4400\text{Å})$; the distribution of R-values has been shown to be bimodal with a minimum at $R=10$, commonly used to define radio-loud (above 10) versus radio-quiet objects. Interestingly, we note that a relevant fraction ($\sim 40\%$) of the BAT AGN is radio-loud and that these objects show a systematically harder X-ray spectra than Seyfert galaxies (mean of 1.66 vs. 2.00). There is large consensus that radio-loud quasars host more massive black holes than radio-quiet ones (e.g. Metcalf & Magliocchetti 2006; McLure & Jarvis 2004). However, there is no simple explanation for this radio-loudness dichotomy. Recently Sikora et al. (2007) showed that the radio-loudness parameter inversely correlates with the Eddington ratio (fraction of bolometric to Eddington luminosity) for both spiral/disk and elliptical galaxies. The fact that spiral-hosted AGN are radio-quiet at high accretion luminosities supports the idea that the black hole spin plays a major role in the jet production (Sikora et al. 2007)⁵. As a confirmation, we find a good correlation of intrinsic X-ray luminosity and radio-loudness (Spearman rank test being 0.57 with probability of 0.003). Such correlation is expected if there is a fundamental connection between accretion and jet activity (Merloni et al. 2003).

⁵ In fact, by merging processes, black holes in elliptical galaxies are expected to have larger spins than those in spiral/disk galaxies.

4. Discussion

We have used the BAT X-ray survey to study key properties of the local ($z \leq 0.1$) AGN population. Our survey is based on the 14-170 keV fluxes and it is sensitive to AGN with column densities up to $N_H \sim 5 \times 10^{24}$ atoms cm^{-2} . Indeed, for a typical source with photon index of 2, the decrease in flux for column densities of $N_H \sim 10^{24}$ atoms cm^{-2} is only $\sim 7\%$ and $\sim 55\%$ ⁶ for column densities of $N_H \sim 3 \times 10^{24}$ atoms cm^{-2} . Thus, we can affirm that this survey is relatively unbiased with respect to photoelectric absorption.

Most of the population synthesis models (Ueda et al. 2003; Treister & Urry 2005; Gilli et al. 2007) predict that Compton-thick AGN ($\log N_H > 24$) provide a significant contribution to the bulk of the CXB emission at 30 keV (Marshall et al. 1980). Although studies of the local Universe (e.g. Risaliti et al., 1999) have shown that Compton-thick objects should be as numerous as moderately obscured AGNs ($\log N_H < 24$) and thus roughly 1/3 of the total AGN population, only a handful of these sources are known (Comastri 2004). Gilli et al. (2007) estimate that the expected fraction of Compton-thick objects at limiting fluxes probed by BAT and INTEGRAL ($\sim 10^{-11}$ erg cm^{-2} s^{-1}) is in the 15–20% range. However the measured fraction of detected Compton-thick objects by these instruments is, so far, close to, or less than, 10% (Markwardt et al. 2005; Beckmann et al. 2006).

The BAT extragalactic sample contains only one source SWIFT J0823.4-0457, which given its colors (see Fig. 1) might be Compton-thick. However, the joint XRT and BAT spectra show that the absorption is below the Compton-thick level ($N_H \sim 10^{23}$ atoms cm^{-2}). We must therefore conclude that no Compton-thick AGN are present in our extragalactic sample. The probability of not detecting Compton-thick objects in a sample of 24 AGN when the expected fraction is 20% (15%) is ~ 0.007 (~ 0.03) while it is 0.1 if the expected fraction is 10%. These probabilities increase (0.03, 0.09 and 0.2 for the 20%, 15% and 10% cases) if we assume that the only source which lacks < 10 keV measurement (J0854.7+1502) is Compton-thick. Thus, the BAT data discard at $> 2\sigma$ level the hypothesis that Compton-thick AGN may represent a fraction of $\sim 20\%$ of the total AGN population.

We find that Sy2s have harder spectra than Sy1s in agreement with what has been deduced from *OSSE*, *BeppoSAX* and *INTEGRAL* data (Zdziarski et al. 2000; Deluit & Courvoisier 2003; Beckmann et al. 2006, respectively). We tested whether this difference could be accounted for by Compton reflection and/or by a high-energy cut-off. We find that the reflection component improves the fit to the Sy1 averaged spectrum (the F-test shows that the reflection is significant at more than the 92% level), but it leaves unaltered the photon index.

⁶Photoelectric absorption as well as Compton scattering has been taken into account in this estimate.

Thus, the difference in photon indices among Sy1s and Sy2s cannot be ascribed solely to orientation effects (a stronger reflection is expected for face-on objects). The spectra of Sy1s show hints of a spectral cut-off at ~ 100 keV in agreement with Deluit & Courvoisier (2003). According to thermal Compton models, the absence of a cut-off in Sy2s might indicate a higher temperature of the Comptonizing medium (with respect to Sy1s) or that non-thermal Compton scattering plays an important role. Nevertheless, given the low S/N of our sources evidences for the cut-off in the Sy1 spectra are weak.

The best power-law fit to the extragalactic source counts distribution yields a slope of $\alpha = 1.55 \pm 0.20$ which is consistent with an Euclidean distribution. From the best fit, we derive a surface density of AGN of $9.6 \pm 1.9 \times 10^{-3} \text{ deg}^{-2}$ above the flux limit of $2 \times 10^{-11} \text{ erg cm}^{-2} \text{ s}^{-1}$; this estimate is in very good agreement, when converted to the 20-40 keV band, with the recently derived source counts distribution based on INTEGRAL data (Beckmann et al. 2006). Beckmann et al. (2006) find a slope of 1.66 ± 0.11 which is also consistent with our measurement, but steeper than the 1.5 Euclidean value. Even though this could be due to a non-perfectly computed sky coverage, the authors suggest that the distribution of AGNs in the local Universe may not be isotropic because of local clustering of sources (e.g. the local group of galaxies).

The BAT source count distribution resolves only 1-2% of the CXB into extragalactic sources; nevertheless as it is unbiased with respect to absorption it gives important information relative to the fraction of obscured sources which are missed by deep < 10 keV surveys because of absorption. The extrapolation of the BAT source count distribution to the 2-10 keV band assuming an unabsorbed spectrum with photon index 2 yields a surface density of AGN of $1.6 \pm 0.32 \times 10^{-2} \text{ deg}^{-2}$ above $10^{-11} \text{ erg cm}^{-2} \text{ s}^{-1}$; while the surface density as extrapolated to brighter fluxes by XMM (Cappelluti et al. 2007) and as predicted by the model of Gilli et al. (2007) is $0.9 \times 10^{-2} \text{ deg}^{-2}$. The factor ~ 2 more sources BAT sees can be explained in term of absorption. Indeed, if we take into account the absorption distribution derived for BAT AGNs by Markwardt et al. (2005) (thus assuming that 66% of all AGN are absorbed with a mean column density of $10^{23} \text{ atoms cm}^{-2}$) we get a surface density $0.86 \pm 0.17 \times 10^{-2} \text{ deg}^{-2}$ which is consistent with the XMM extrapolation and the model prediction.

The extragalactic sample is composed of $\sim 90\%$ emission-line galaxies and $\sim 10\%$ blazars. We find that 55% of the emission-line galaxies are obscured by absorbing columns larger than $10^{22} \text{ H-atoms cm}^{-2}$. This fraction is in agreement with the INTEGRAL measurements (e.g. Sazonov et al. 2007), but less than what is suggested ($\sim 75\%$) by the unified AGN model. However, Sazonov et al. (2007) successfully showed that low-luminosity (mostly absorbed) AGN account for much, $\sim 90\%$, of the luminosity density of the local Universe. This is

also confirmed by the model of Gilli et al. (2007) which shows that the required fraction of obscured sources varies with intrinsic luminosity being 3.7 and 1.0 below and above $10^{43.5}$ erg s^{-1} . A relevant fraction ($\sim 40\%$) of the BAT-detected AGN is radio-loud. These objects show a systematically harder X-ray spectra than Seyfert galaxies (1.66 vs. 2.00). The hard photon index and the correlation of radio-loudness with X-ray luminosity suggest that a jet is presently at work in all these objects. Our sample also comprises 1 (and possibly up to 3 considering the ROSAT lower limits on the absorption) highly luminous highly absorbed QSO.

5. Summary

We use the *Swift*/BAT instrument to study the properties of the local ($z \leq 1$) AGN in connection with the synthesis of the X-ray background emission. The results of this study can be summarized as follows:

- Despite the consensus that Compton-thick objects may represent a substantial fraction of the local AGN population (e.g. Risaliti et al. 1999; Gilli et al. 2007), we do not detect any such object. The probability associated to this non-detection is 0.007, 0.03 and 0.1 when assuming that their fraction should be 20%, 15% and 10% of the total AGNs. BAT discards at $> 2\sigma$ the hypothesis that the fraction of Compton-thick objects is 20%.
- Seyfert 2 galaxies have harder X-ray spectra than Seyfert 1. We find that this difference cannot be ascribed solely to the different viewing angle and thus to the different amount of Compton reflection which is expected. The Seyfert 1 galaxies comprised in our sample show weak evidences for a spectral cut-off in the ~ 100 keV range. This might highlight an intrinsic difference among the two classes. Indeed, the absence of a cut-off in the spectra of Seyfert 2s might indicate a different (higher) temperature of the Comptonizing medium or that non-thermal Compton scattering play an important role.
- The best power-law fit to the extragalactic source counts is consistent with a Euclidean function with slope of 1.55 ± 0.20 . At the current limiting fluxes (2×10^{-11} erg $cm^{-2} s^{-1}$), BAT resolves only 1–2% of the CXB emission in the 14–170 keV band.
- The fraction of emission-line AGN which is absorbed by $N_H > 10^{22}$ atoms cm^{-2} is $\sim 55\%$. This is lower than the 75% expected by the standard AGN unified model.

This work shows the capabilities of BAT to produce an unbiased sample of AGN which is important for the understanding of the synthesis of the CXB emission in the hard X-ray band.

MA acknowledges N. Gehrels and the BAT team for hospitality, M. Capalbi for assistance during Beppo-SAX and Swift-XRT data analysis, N. Cappelluti for useful discussions on the source count distribution derivation, R. Mushotzky for valuable suggestions and the anonymous referee for his comments which helped improving the paper. This research has made use of the NASA/IPAC extragalactic Database (NED) which is operated by the Jet Propulsion Laboratory, of data obtained from the High Energy Astrophysics Science Archive Research Center (HEASARC) provided by NASA's Goddard Space Flight Center, of the SIMBAD Astronomical Database which is operated by the Centre de Données astronomiques de Strasbourg, of the Sloan Digital Sky Survey (SDSS) managed by the Astrophysical Research Consortium (ARC) for the Participating Institutions and of the ROSAT All Sky Survey maintained by the Max Planck Institut für Extraterrestrische Physik.

REFERENCES

- Ajello, M., Greiner, J., Kanbach, G., Rau, A., Strong, A. W., & Kennea, J. A. 2007, *ApJ*, submitted
- Ajello, M., Greiner, J., Rau, A., Barthelmy, S., Kennea, J. A., Falcone, A., Godet, O., Grupe, D., Tueller, J., Markwardt, C., Mushotsky, R., Belloni, T., Mukai, K., Holland, S. T., & Gehrels, N. 2006, *The Astronomer's Telegram*, 697, 1
- Antonucci, R. 1993, *ARA&A*, 31, 473
- Arnaud, K. A. 1996, in *Astronomical Society of the Pacific Conference Series*, Vol. 101, *Astronomical Data Analysis Software and Systems V*, ed. G. H. Jacoby & J. Barnes, 17–+
- Avni, Y. & Bahcall, J. N. 1980, *ApJ*, 235, 694
- Barthelmy, S. D., Barbier, L. M., Cummings, J. R., Fenimore, E. E., Gehrels, N., Hullinger, D., Krimm, H. A., Markwardt, C. B., Palmer, D. M., Parsons, A., Sato, G., Suzuki, M., Takahashi, T., Tashiro, M., & Tueller, J. 2005, *Space Science Reviews*, 120, 143
- Bassani, L., Dadina, M., Maiolino, R., Salvati, M., Risaliti, G., della Ceca, R., Matt, G., & Zamorani, G. 1999, *ApJS*, 121, 473

- Beckmann, V., Soldi, S., Shrader, C. R., Gehrels, N., & Prodit, N. 2006, *ApJ*, 652, 126
- Bird, A. J., Barlow, E. J., Bassani, L., Bazzano, A., Bélanger, G., Bodaghee, A., Capitanio, F., Dean, A. J., Flocchi, M., Hill, A. B., Lebrun, F., Malizia, A., Mas-Hesse, J. M., Molina, M., Moran, L., Renaud, M., Sguera, V., Shaw, S. E., Stephen, J. B., Terrier, R., Ubertini, P., Walter, R., Willis, D. R., & Winkler, C. 2006, *ApJ*, 636, 765
- Bolton, J. G. & Butler, P. W. 1975, *Australian Journal of Physics Astrophysical Supplement*, 34, 33
- Cappelluti, N., Hasinger, G., Brusa, M., Comastri, A., Zamorani, G., Boehringer, H., Brunner, H., Civano, F., Finoguenov, A., Fiore, F., Gilli, R., Griffiths, R. E., Mainieri, V., Matute, I., Miyaji, T., & Silverman, J. 2007, *ArXiv e-prints*, 704
- Comastri, A. 2004, in *Astrophysics and Space Science Library*, Vol. 308, *Astrophysics and Space Science Library*, ed. A. J. Barger, 245–+
- Comastri, A., Setti, G., Zamorani, G., & Hasinger, G. 1995, *A&A*, 296, 1
- Crawford, C. S. & Fabian, A. C. 1995, *MNRAS*, 273, 827
- Crawford, D. F., Jauncey, D. L., & Murdoch, H. S. 1970, *ApJ*, 162, 405
- Deluit, S. & Courvoisier, T. J.-L. 2003, *A&A*, 399, 77
- den Hartog, P. R., Hermsen, W., Kuiper, L. M., in’t Zand, J. J. M., Winkler, C., & Domingo, A. 2004, *The Astronomer’s Telegram*, 261, 1
- Elvis, M., Plummer, D., Schachter, J., & Fabbiano, G. 1992, *ApJS*, 80, 257
- Evans, I. N., Ford, H. C., Kinney, A. L., Antonucci, R. R. J., Armus, L., & Caganoff, S. 1991, *ApJ*, 369, L27
- Fenimore, E. E. & Cannon, T. M. 1978, *Appl. Opt.*, 17, 337
- Gehrels, N., Chincarini, G., Giommi, P., Mason, K. O., Nousek, J. A., Wells, A. A., White, N. E., Barthelmy, S. D., Burrows, D. N., Cominsky, L. R., Hurley, K. C., Marshall, F. E., Mészáros, P., Roming, P. W. A., Angelini, L., Barbier, L. M., Belloni, T., Campana, S., Caraveo, P. A., Chester, M. M., Citterio, O., Cline, T. L., Cropper, M. S., Cummings, J. R., Dean, A. J., Feigelson, E. D., Fenimore, E. E., Frail, D. A., Fruchter, A. S., Garmire, G. P., Gendreau, K., Ghisellini, G., Greiner, J., Hill, J. E., Hunsberger, S. D., Krimm, H. A., Kulkarni, S. R., Kumar, P., Lebrun, F., Lloyd-Ronning, N. M., Markwardt, C. B., Mattson, B. J., Mushotzky, R. F., Norris, J. P.,

- Osborne, J., Paczynski, B., Palmer, D. M., Park, H.-S., Parsons, A. M., Paul, J., Rees, M. J., Reynolds, C. S., Rhoads, J. E., Sasseen, T. P., Schaefer, B. E., Short, A. T., Smale, A. P., Smith, I. A., Stella, L., Tagliaferri, G., Takahashi, T., Tashiro, M., Townsley, L. K., Tueller, J., Turner, M. J. L., Vietri, M., Voges, W., Ward, M. J., Willingale, R., Zerbi, F. M., & Zhang, W. W. 2004, *ApJ*, 611, 1005
- Giacconi, R., Gursky, H., Paolini, F. R., & Rossi, B. B. 1962, *Physical Review Letters*, 9, 439
- Gilli, R., Comastri, A., & Hasinger, G. 2007, *A&A*, 463, 79
- Gilli, R., Salvati, M., & Hasinger, G. 2001, *A&A*, 366, 407
- Giommi, P., Tagliaferri, G., Beuermann, K., Branduardi-Raymont, G., Brissenden, R., Graser, U., Mason, K. O., Mittaz, J. D. P., Murdin, P., Pooley, G., Thomas, H.-C., & Tuohy, I. 1991, *ApJ*, 378, 77
- Götz, D., Mereghetti, S., Merlini, D., Sidoli, L., & Belloni, T. 2006, *A&A*, 448, 873
- Gruber, D. E., Matteson, J. L., Peterson, L. E., & Jung, G. V. 1999, *ApJ*, 520, 124
- Guainazzi, M., Matt, G., & Perola, G. C. 2005, *A&A*, 444, 119
- Jonker, P. G., van der Klis, M., Homan, J., Méndez, M., van Paradijs, J., Belloni, T., Kouveliotou, C., Lewin, W., & Ford, E. C. 2001, *ApJ*, 553, 335
- Landi, R., Masetti, N., Morelli, L., Palazzi, E., Bassani, L., Malizia, A., Bazzano, A., Bird, A. J., Dean, A. J., Galaz, G., Minniti, D., & Ubertini, P. 2007, *ArXiv e-prints*, 706
- Laor, A. 2000, *ApJ*, 543, L111
- Magdziarz, P. & Zdziarski, A. A. 1995, *MNRAS*, 273, 837
- Malizia, A., Malaguti, G., Bassani, L., Cappi, M., Comastri, A., Di Cocco, G., Palazzi, E., & Vignali, C. 2002, *A&A*, 394, 801
- Markwardt, C. B., Tueller, J., Skinner, G. K., Gehrels, N., Barthelmy, S. D., & Mushotzky, R. F. 2005, *ApJ*, 633, L77
- Marshall, F. E., Boldt, E. A., Holt, S. S., Miller, R. B., Mushotzky, R. F., Rose, L. A., Rothschild, R. E., & Serlemitsos, P. J. 1980, *ApJ*, 235, 4
- Masetti, N., Bassani, L., Dean, A. J., Ubertini, P., & Walter, R. 2006a, *The Astronomer's Telegram*, 735, 1

- Masetti, N., Morelli, L., Palazzi, E., Galaz, G., Bassani, L., Bazzano, A., Bird, A. J., Dean, A. J., Israel, G. L., Landi, R., Malizia, A., Minniti, D., Schiavone, F., Stephen, J. B., Ubertini, P., & Walter, R. 2006b, *A&A*, 459, 21
- Matt, G., Guainazzi, M., Frontera, F., Bassani, L., Brandt, W. N., Fabian, A. C., Fiore, F., Haardt, F., Iwasawa, K., Maiolino, R., Malaguti, G., Marconi, A., Matteuzzi, A., Molendi, S., Perola, G. C., Piraino, S., & Piro, L. 1997, *A&A*, 325, L13
- Matt, G., Guainazzi, M., & Maiolino, R. 2003, *MNRAS*, 342, 422
- McLure, R. J. & Jarvis, M. J. 2004, *MNRAS*, 353, L45
- Merloni, A., Heinz, S., & di Matteo, T. 2003, *MNRAS*, 345, 1057
- Metcalfe, R. B. & Magliocchetti, M. 2006, *MNRAS*, 365, 101
- Norton, A. J., Beardmore, A. P., Retter, A., & Buckley, D. A. H. 2000, *MNRAS*, 312, 362
- Rau, A., Greiner, J., Salvato, M., & Ajello, M. 2007, *A&A*, submitted
- Revnivtsev, M., Sazonov, S., Churazov, E., & Trudolyubov, S. 2006, *A&A*, 448, L49
- Risaliti, G., Maiolino, R., & Salvati, M. 1999, *ApJ*, 522, 157
- Sazonov, S., Revnivtsev, M., Krivonos, R., Churazov, E., & Sunyaev, R. 2007, *A&A*, 462, 57
- Schmidt, M. 1968, *ApJ*, 151, 393
- Schwabe, A., Hasinger, G., Lehmann, I., Schwarz, R., Brunner, H., Neizvestny, S., Ugryumov, A., Balega, Y., Trümper, J., & Voges, W. 2000, *Astronomische Nachrichten*, 321, 1
- Sikora, M., Stawarz, Ł., & Lasota, J.-P. 2007, *ApJ*, 658, 815
- Slowikowska, A., Kanbach, G., Borkowski, J., & Becker, W. 2006, On the Present and Future of Pulsar Astronomy, 26th meeting of the IAU, Joint Discussion 2, 16-17 August, 2006, Prague, Czech Republic, JD02, #8, 2
- Sowards-Emmerd, D., Romani, R. W., Michelson, P. F., & Ulvestad, J. S. 2004, *ApJ*, 609, 564
- Treister, E. & Urry, C. M. 2005, *ApJ*, 630, 115

- Tueller, J., Barthelmy, S., Burrows, D., Falcone, A., Gehrels, N., Grupe, D., Kennea, J., Markwardt, C. B., Mushotzky, R. F., & Skinner, G. K. 2005, *The Astronomer's Telegram*, 669, 1
- Ueda, Y., Akiyama, M., Ohta, K., & Miyaji, T. 2003, *ApJ*, 598, 886
- Voges, W., Aschenbach, B., Boller, T., Bräuninger, H., Briel, U., Burkert, W., Dennerl, K., Englhauser, J., Gruber, R., Haberl, F., Hartner, G., Hasinger, G., Kürster, M., Pfeffermann, E., Pietsch, W., Predehl, P., Rosso, C., Schmitt, J. H. M. M., Trümper, J., & Zimmermann, H. U. 1999, *A&A*, 349, 389
- Worsley, M. A., Fabian, A. C., Bauer, F. E., Alexander, D. M., Hasinger, G., Mateos, S., Brunner, H., Brandt, W. N., & Schneider, D. P. 2005, *MNRAS*, 357, 1281
- Zamorani, G., Henry, J. P., Maccacaro, T., Tananbaum, H., Soltan, A., Avni, Y., Liebert, J., Stocke, J., Strittmatter, P. A., Weymann, R. J., Smith, M. G., & Condon, J. J. 1981, *ApJ*, 245, 357
- Zdziarski, A. A., Poutanen, J., & Johnson, W. N. 2000, *ApJ*, 542, 703

A. Spectral extraction method

We have developed a method to extract the averaged long term spectrum of a source. In this method, the spectrum is obtained as a weighted average of the source spectra of all observations where the source is in the field of view. In particular, the averaged source count rates in the i -th energy channel, \bar{R}_i , and their error $\bar{\sigma}_i$, are given by the following equations:

$$\bar{R}_i = \frac{\sum_{j=0}^N r_j * w_j}{\sum_{j=0}^N w_j}, \quad \bar{\sigma}_i = \sqrt{\frac{\sum_{j=0}^N w_j V_j}{N \sum_{j=0}^N w_j}} \quad (\text{A1})$$

where r_j is the source count rate in the j -th observation, w_j is the weight used and the sums extend over all observations which contain the source. Using the inverse of the count rate variance V_j as a weight, the previous equations simplify to:

$$\bar{R}_i = \frac{\sum_{j=0}^N r_j \cdot 1/V_j}{\sum_{j=0}^N 1/V_j}, \quad \bar{\sigma}_i = \sqrt{\frac{1}{\sum_{j=0}^N 1/V_j}} \quad (\text{A2})$$

However, the spectra entering in Eq. A2 must be corrected for off-axis count rate variation and for residual background contamination. We explain below the way these corrections are implemented.

A.1. Rate variation as a function of off-axis angle

The detected count rates strongly vary with the position of the source in the FOV; a source at the far edge of the partially coded FOV (PCFOV) can experience a decrease in rate of a factor 2 (depending also on energy) when compared to its on-axis rate.

The standard Swift-BAT imaging software corrects for geometrical off-axis effects like cosine and partial coding (vignetting) effects; it is only when the response matrix is generated (tool *batdrngen*) that other effects like detector thickness and effective area variation are taken into account.

Since in equation A2 we are averaging over spectra at different positions in the FOV, we need to take into account the variations in the rates produced by the detector response. In order to do so, we have analyzed a series of more than 1000 Crab observations. For each of our 6 energy channels we made a polynomial fit to the Crab rate as a function of the off-axis angle, and derived a set of corrective coefficients. These coefficients are then used to correct the rates of each source spectrum in order to transform them to the equivalent on-axis rates. The variation of the Crab rates as a function of position in the FOV is reported in Fig. 6.

A.2. Residual background contamination

In order to extract a source spectrum from survey data (in form of Detector Plane Histograms, DPH) the user must first produce a mask of weights (tool *batmaskwtimg*) for the source position and then use this mask to extract the detected counts from the array (tool *batbinevt*). The weights are chosen such that the resulting spectrum is already background-subtracted. This is an implementation of the standard mask weighting technique called *balanced correlation* (Fenimore & Cannon 1978). The automatic background subtraction works as long as the noise in the array is flat and not correlated with the mask pattern. These conditions are not always satisfied and a small background contamination can arise.

The total background contamination for the case of the Crab is $< 2\%$ when compared to the Crab on-axis rate in the 14-195 keV band. Thus, this contamination does not pose problems for bright sources. However, it becomes relevant for the spectral analysis of faint objects with intensities of $\sim m\text{Crab}$.

In order to correct for this residual background contamination, we fit the *batclean* background model to each energy channel in order to create a background prediction for each of them. Convoluting these background predictions with the mask of weights generated for the source under analysis yields the residual background term which the mask weighting technique did not manage to suppress.

A.3. Spectral fitting

The final source rates in the i -th energy channel are computed as:

$$\bar{R}_i = \frac{\sum_{j=0}^N (r_j - b_j) \cdot K(E, \theta) \cdot 1/V_j}{\sum_{j=0}^N 1/V_j} \quad (\text{A3})$$

where b_j is the residual background term, $K(E, \theta)$ is the parametrized instrumental response as function of the energy channel and the off-axis angle and V_j is the rate variance. The weighted averaged spectrum is then input, together with a the BAT response matrix, to XSPEC 11.3.2 (Arnaud 1996) for spectral fitting.

Finally, we checked that the averaged Crab spectrum, obtained with the above method, is consistent with the standard (BAT) Crab spectrum as detected in each observation (photon index of 2.15 and normalization of 10.15 photons $\text{cm}^{-2} \text{s}^{-1}$ at 1 keV in the 15–200 keV energy range).

A.4. Notes on individual sources

We report a brief description of the source spectra for all new, or interesting, sources found in this analysis. All quoted errors are 90%. The spectra of all the sources are reported in Figures 7, 8, 9, 10, 11, 12, 13 and 13 (available online).

3C 105.0 is a Sy2 galaxy. The BAT and XRT data can be fitted by an absorbed power law model with photon index of 1.65 ± 0.13 and hydrogen column density of $29.4_{-4.8}^{+5.7} \times 10^{22}$ atoms cm^{-2} . Given its absorption and its luminosity (4.45×10^{44} erg s^{-1}), 3C 105.0 is a highly-absorbed highly-luminous QSO.

1 AXG J042556-5711 (also known as 1H 0419-577LB 1727, 1ES 0425-573 and IRAS F04250-5718) is a radio-quiet Seyfert galaxy which has been observed over recent years by ASCA, ROSAT, BeppoSAX and recently also by XTE (Revnivtsev et al. 2006). The ASCA and BAT data are well fit by an unabsorbed cut-off power-law model with photon index of 1.54 ± 0.028 and cut-off at $73_{-24.1}^{+46.2}$ keV.

3C 120 is a Sy1 galaxy. This source was observed by ASCA. The best fit to ASCA and BAT data is an absorbed power law model with absorption consistent with the galactic one and photon index $1.80_{-0.04}^{+0.04}$ and a black body component with a temperature of $0.27_{-0.025}^{+0.026}$ keV.

MCG -01-13-025 is a Sy1.2 (in NED, but Sy1 in SIMBAD) galaxy detected in soft X-rays by ROSAT (Voges et al. 1999). The BAT spectrum is consistent with a power law with photon index of $1.6_{-0.47}^{+0.48}$ and it extends up to 200 keV.

SWIFT J0505.7-2348, also known as XSS J05054-2348 (Revnivtsev et al. 2006) is a Sy2 galaxy. When combining both XRT and BAT data for this source we get an intrinsic, rest frame, absorption of $4.8_{-0.7}^{+0.9} \times 10^{22}$ atoms cm^{-2} and a photon index of $1.77_{-0.07}^{+0.08}$.

CSV 6150, also known as IRAS 05078+1626, is cataloged as Sy1 in SIMBAD and as Sy1.5 in NED. The BAT spectrum can be fitted with a power law with photon index of $1.94_{-0.23}^{+0.25}$. The source flux in the 14–170 keV band is $6.3_{-4.0}^{+0.7} \times 10^{-11}$ erg cm^{-2} s^{-1} while the luminosity is $4.4_{-2.2}^{+0.6} \times 10^{43}$ erg s^{-1} .

4U 0513-40 is a low mass X-ray binary detected in X-rays by EXOSAT (Giommi et al. 1991). The BAT spectrum can be fit by a bremsstrahlung model with temperature of $29.7_{-5.8}^{+7.5}$ keV.

QSO B0513-002 is a Sy1 galaxy. The BAT and ASCA spectra can be fitted by an absorbed power-law model and a black body component. The required absorption is in agreement with the galactic one. The photon index and the plasma temperature are respectively $1.83^{+0.02}_{-0.016}$ and $0.27^{+0.02}_{-0.02}$ keV. We also detect a an iron line whose equivalent width is $90.8^{+66.2}_{-76.7}$ eV.

SWIFT J0517.1+1633 is a new hard X-ray source (Ajello et al. 2007). The BAT spectrum is best fit by a power law model with photon index of $2.0^{+0.23}_{-0.26}$.

ESO 362- G 018 is a Sy1 galaxy detected at hard X-ray by BAT (Tueller et al. 2005). The BAT and XRT data are best fit by an absorbed power-law model with photon index of $1.50^{+0.03}_{-0.02}$ and absorption consistent with the galactic value.

Pictor A is a radio-loud Sy1 galaxy initially detected in X-ray by the EINSTEIN observatory (Elvis et al. 1992). The best fit to ASCA and BAT data is an absorbed power-law model with photon index of $1.8^{+0.02}_{-0.02}$ and intrinsic absorption of $1.14^{+0.01}_{-0.05} \times 10^{21}$ atoms cm^{-2} slightly in excess of the galactic one (4×10^{20} atoms cm^{-2}).

ESO 362-G021 is a BL Lac object. ASCA and XRT data are available for this source. The best fit to ASCA, BAT and XRT data is an absorbed power law with photon index of $1.72^{+0.04}_{-0.04}$ and intrinsic column density of $0.14^{+0.02}_{-0.02} \times 10^{22}$ atoms cm^{-2} .

TV Col is a DQ Her type cataclysmic variable already detected at soft and hard X-rays. A power law fit to the BAT spectrum does not yield acceptable results; instead a bremsstrahlung model with a plasma temperature of $28.2^{+4.6}_{-3.8}$ keV fits the data well.

TW PIC is a cataclysmic variable of the DQ Her type (Norton et al. 2000). The BAT spectrum is best fitted by a bremsstrahlung model with a plasma temperature of $13.5^{+10.6}_{-5.6}$ keV. The flux of 5.5×10^{-12} erg cm^{-2} s^{-1} in the 20-40 keV band is a factor 2 lower than the one reported in a recent INTEGRAL measurement (Götz et al. 2006) suggesting variability.

LMC X-3 is high mass X-ray binary (HXB). The BAT spectrum is consistent with a power law whose photon index is $2.0^{+0.4}_{-0.3}$.

LMC X-1 is a well known black hole candidate. It is detected up to 200 keV with a steep photon index of $2.3^{+0.22}_{-0.20}$. The flux is a factor 2 lower than the one measured by INTEGRAL (Götz et al. 2006), suggesting variability.

PSR B0540-69.3 is a young rotation-powered pulsar recently detected up to 60 keV also by

INTEGRAL (Götz et al. 2006; Slowikowska et al. 2006). The Pulsar is detected in BAT up to 200 keV and its spectrum can be modeled as a power law with photon index of $1.85_{-0.26}^{+0.28}$.

PKS 0537-286 at $z=3.1$ is one of the most luminous high-redshift quasar. Recognized first as a radio source (Bolton & Butler 1975) it was discovered in X-rays by the Einstein observatory (Zamorani et al. 1981) and then studied by ROSAT, ASCA and lately by XMM. The BAT detection in hard X-rays is the first to date, however there is a claim that PKS 0537-286 be the MeV counterpart of the EGRET source 3EG J0531-2940 (Sowards-Emmerd et al. 2004). A joint spectral fit to XRT and BAT data reveals an exceptionally hard spectral slope of $1.35_{-0.08}^{+0.06}$.

PKS 0548-322 is a well known blazar already detected in hard X-rays (see for example Donato et al., 2005). A joint spectrum of XRT and BAT data with an absorbed power law model yields a photon index of $1.8_{-0.03}^{+0.03}$ and an intrinsic absorption of $2.57_{-0.5}^{+0.6} \times 10^{20}$ atoms cm^{-2} .

NGC 2110 is a well known Sy2 galaxy. The BAT, ASCA and XRT data can be fit by an absorbed power law model (photon index of $1.62_{-0.01}^{+0.01}$ and intrinsic hydrogen column density of $4.0_{-0.07}^{+0.13} \times 10^{22}$ atoms cm^{-2}) with a soft excess which could be described as black body component with temperature of $0.47_{-0.02}^{+0.02}$. We also detected an unresolved Fe K_{α} of equivalent width of 118_{-53}^{+42} eV.

LEDA 75476, also known as 3A 0557-383, EXO 055620-3820.2 and CTS B31.01, is a Sy1 galaxy. The BAT spectrum is consistent with a power law model with photon index of 2.0 ± 0.4 . The ASCA and BAT are well fit by an absorbed power law model with photon index of $1.74_{-0.03}^{+0.02}$ and intrinsic absorbing column density of $2.2_{-0.13}^{+0.11} \times 10^{22}$ atoms cm^{-2} . A clear excess below 2 keV is detected in the ASCA data and this can be modeled as a black body component with a temperature of $0.28_{-0.05}^{+0.08}$ keV. A Fe K_{α} line is also required by the fit (F-test yielding a probability of the line being spurious of 10^{-8}) and its equivalent width is 0.132 keV. The reduced χ^2 of the overall fit is 1.1.

ESO 490-G 26 is a Sy1.2 galaxy. The joint XRT-BAT spectrum can be described as a power law with photon index of $1.90_{-0.04}^{+0.05}$ and an intrinsic, in addition to the galactic, absorption of $2.7_{-0.05}^{+0.05} \times 10^{21}$ atoms cm^{-2} . The flux and the luminosity in the 14–170 keV band are $3.6_{-1.3}^{+1.1} \times 10^{-11}$ erg cm^{-2} s^{-1} and $4.7_{-3.6}^{+1.2} \times 10^{43}$ erg s^{-1} .

SWIFT J0727.5-2406 has a spectrum consistent with a power law model with photon index of 1.53 ± 0.54 . As already noted by Rau et al. (2007) this BXS source is likely asso-

ciated with the nearby ROSAT source 1RXS J072720.8-240629 and with the radio object NVSS J072721-240632.

V441 Pup is a high mass X-ray binary where the companion was optically identified as a Be star. The BAT spectrum is very steep and it can either be fitted by a power law with a photon index of 4.5 ± 1.5 or by a bremsstrahlung model with a plasma temperature of $12.4_{-5.6}^{+13.6}$ keV.

BG CMi is a well known intermediate polar. The BAT spectrum is consistent with a bremsstrahlung model with a plasma temperature of $31.3_{-14.2}^{+41.2}$ keV.

SWIFT J0732.5-1331 was detected for the first time by BAT in hard X-rays (Ajello et al. 2006). It was then identified as a new intermediate polar (Wheatley et al. 2006 and references therein). The BAT spectrum is consistent with a bremsstrahlung model with a plasma temperature of $33.2_{-14.2}^{+50.1}$ keV.

SWIFT J0739.6-3144 is a newly discovered hard X-ray source (Ajello et al. 2007), recently identified as a Sy2 galaxy (Rau et al. 2007). A simple power law fit to the BAT spectrum yields a photon index of $1.77_{-0.43}^{+0.51}$. We also estimated the lower limit on the absorbing column density considering the undetection by ROSAT; this limit is $\sim 2 \times 10^{22}$ atoms cm^{-2} . The flux and the luminosity in the 14–170 keV band are $2.3_{-1.8}^{+1.1} \times 10^{-11}$ erg cm^{-2} s^{-1} and $3.2_{-1.9}^{+1.6} \times 10^{43}$ erg s^{-1} .

SWIFT J0743.0-2543 is a newly discovered hard X-ray source (Ajello et al. 2007). The BAT spectrum is consistent with a power-law model with photon index of $1.78_{-0.56}^{+0.69}$. As noted in Rau et al. (2007) this BXS source is likely to be associated with the ROSAT source 1RXS J074315.6-254545 and the galaxy LEDA 86073.

IGR J07597-3842 is a source first detected by INTEGRAL in the VELA region (den Hartog et al. 2004). It was identified as being a Sy1.2 (Masetti et al. 2006b). This source was also observed by XRT and when jointly fitting XRT and BAT data we get that the best fit is an absorbed power law with photon index of $1.8_{-0.07}^{+0.08}$ and column density of $5.8_{-0.5}^{+0.5} \times 10^{21}$ atoms cm^{-2} consistent with the galactic foreground absorption. The source is thus unabsorbed. The flux and the luminosity in the 14–170 keV band are $4.2_{-2.4}^{+0.6} \times 10^{-11}$ erg cm^{-2} s^{-1} and $15.9_{-14.8}^{+1.5} \times 10^{43}$ erg s^{-1} .

UGC 4203 is a Sy2 galaxy. As already noted in Matt et al. (2003), this source shows transitions between a reflection-dominated and a transmission-dominated spectrum. The ASCA

and BAT data can be successfully fit by a reflection model (PEXRAV, Magdziarz & Zdziarski 1995) with photon index of 1.68 ± 0.1 and a reflection normalization of $65.2_{-23.07}^{+43.2}$ and a prominent iron line with equivalent width of $0.7_{-0.6}^{+1.1}$ keV. A soft excess at energies < 1 keV can be modeled as a black body component with a temperature of $0.3_{-0.05}^{+0.08}$ keV.

XRT data are also available for this source. However, the XRT spectrum has a lower quality than the ASCA one. In the XRT observation, the source is found in a transmission-dominated state; the best fit model is an absorbed reflection model (the reflection component is required by the BAT spectrum) with hydrogen column density of $N_H = 12.5_{-3.7}^{+5.0} \times 10^{22}$ atoms cm^{-2} , photon index of $2.0_{-0.25}^{+0.25}$ and reflection normalization of $2.12_{-1.5}^{+2.5}$.

SWIFT J0811.5+0937 is a new BXS source detected in Ajello et al. (2007). The BAT spectrum is consistent with a power law with photon index of $2.2_{-0.9}^{+2.1}$. Rau et al. (2007) identified RX J081132.4+093403 as possible counterpart. Optical spectroscopy revealed that this source is a candidate X-ray Bright Optically Normal Galaxy (XBONG). If we extrapolate the BAT power law to the ROSAT-PSPC energy band (0.1–2.4 keV) we get no indication of intrinsic absorption.

SWIFT J0823.4-0457 is a source detected for the first time in hard X-rays by BAT and associated, during an XRT follow-up, with the galaxy FAIRALL 0272 (Ajello et al. 2007). An optical follow-up showed that the source is a Sy2 (Masetti et al. 2006a). XRT and BAT data are best fit by a highly absorbed power law. The photon index is $1.84_{-0.22}^{+0.28}$ and the absorbing column density is $19.3_{-5.4}^{+6.8} \times 10^{22}$ atoms cm^{-2} .

Vela PSR has a spectrum consistent with a power law whose photon index is 1.88 ± 0.2 .

FRL 1146 is a Sy1 galaxy detected in hard X-ray by INTEGRAL (Bird et al. 2006). The BAT spectrum is characterized by a power law with photon index of $1.88_{-0.31}^{+0.37}$ extending up to 200 keV. The 14–170 keV flux and luminosity of $3.3_{-0.7}^{+0.8} \times 10^{-11}$ erg cm^{-2} s^{-1} and $7.2_{-1.4}^{+1.6} \times 10^{43}$ erg s^{-1} are in agreement with the INTEGRAL measurement. FRL 1146 was also detected in the ROSAT all-sky survey at 12 count s^{-1} , considering the extrapolation of the BAT power law to the ROSAT band yields ~ 8 count s^{-1} so it is very likely that the source is unabsorbed.

3C 206 is a narrow line, radio loud, QSO detected for the first time in hard X-rays (> 20 keV). It was detected by Lawson & Turner (1997) using GINGA in the 2-10 keV. The BAT spectrum is consistent with a pure power-law model with photon index of $1.95_{-0.39}^{+0.43}$. 3C 206 was detected by the ROSAT PSPC with 0.37 ct s^{-1} during the all-sky survey (Voges et al. 1999); if we use the BAT power law spectrum and we extrapolate it to the 0.1-2.4 keV band, we

get that no additional absorption (with respect to the galactic one) is required to match the observed ROSAT count rate.

SWIFT J0844.9-3531 is a new hard X-ray source detected in Ajello et al. (2007). The BAT spectrum is consistent with a power law model with photon index $1.91_{-0.68}^{+0.46}$. The flux in the 14–170 keV band is $1.7_{-0.6}^{+1.1} \times 10^{-11}$ erg cm⁻² s⁻¹. Rau et al. (2007) noted that this BXS source might likely be associated with the ROSAT source 1RXS J084521.7-353048.

SWIFT J0854.7+1502 is a new hard X-ray source detected in Ajello et al. (2007) and identified in Rau et al. (2007) as a Sy2 galaxy. It has a flat spectrum which can be modeled as a power law with photon index $1.41_{-0.9}^{+0.7}$. A lower limit on the absorbing column density of 5×10^{21} atoms cm⁻² can be derived by the non-detection of this source in the ROSAT all-sky survey.

SWIFT J0917.2-6221 is a new hard X-ray source. We analyzed a 7 ks XRT observation of this source. The XRT and BAT data are well fit by an absorbed power law model whose photon index is $1.87_{-0.04}^{+0.07}$ and absorbing column density of $1.33_{-0.10}^{+0.18} \times 10^{22}$ atoms cm⁻². A clear excess is present at energies <1 keV and this can be well described as a black body component peaking at 0.14 keV. The flux and the luminosity in the 14–170 keV band are $2.6_{-0.8}^{+0.8} \times 10^{-11}$ erg cm⁻² s⁻¹ and $20.0_{-5.0}^{+6.0} \times 10^{43}$ erg s⁻¹.

Mrk 0704, or SWIFT 0918.5+1618, is another source found thanks to our algorithm (Ajello et al. 2007). During an XRT follow-up, the galaxy Mrk 704 was found as the BAT counterpart. Mrk 704 was previously detected in soft X-rays by ROSAT (Schwope et al. 2000). In a recent optical follow-up, the galaxy was found to be a Sy1 (Masetti et al. 2006a). We have analyzed ASCA, XRT and BAT data for this source. The best fit to the three datasets is a partial covering model where the covering fraction is 0.5 and the powerlaw photon index is $1.36_{-0.07}^{+0.10}$. The source is highly absorbed with a column density of $1.5_{-0.3}^{+0.6} \times 10^{23}$ atoms cm⁻². We also detected an iron line whose equivalent width is 160 eV.

4U 0919-54, detected at very high significance, is a LMXB also known to produce X-ray bursts (Jonker et al. 2001). Its spectrum is characterized by a steep photon index of 2.35 ± 0.25 , alternatively a bremsstrahlung model with a plasma temperature of $45.11_{-9.80}^{+26.13}$ keV yields a better χ^2 .

MCG -01-24-012 is a Sy2 galaxy already detected in hard X-rays by Beppo-SAX (Malizia et al. 2002). When fitting both XRT and BAT data we get that the spectrum is consistent with an absorbed power law whose photon index is $1.7_{-0.07}^{+0.08}$ and intrinsic absorption is

$6.5_{-0.7}^{+0.8} \times 10^{22}$ atoms cm^{-2} .

NGC 2992 is a Sy 1.9. The best fit for combined XRT, ASCA and BAT data is an absorbed power law with photon index of $1.24_{-0.05}^{+0.06}$ and intrinsic hydrogen column density of $0.17_{-0.03}^{+0.03} \times 10^{22}$ atoms cm^{-2} . We also detected the presence of an unresolved Fe K_{α} line whose equivalent width is $0.52_{-0.1}^{+1.0}$ keV in agreement with an old Beppo-Sax measurement (Gilli et al. 2001) where the reported column density is 1×10^{22} atoms cm^{-2} .

ESO 434-G 040 is a known Sy2 galaxy recently detected in hard X-rays also by INTEGRAL (Bird et al. 2006). A joint fit to ASCA, XRT and BAT data with an absorbed power law model yields a photon index of $1.77_{-0.07}^{+0.006}$ and a column density of $1.5_{-0.09}^{+0.026} \times 10^{22}$ atoms cm^{-2} . A clear excess below 2 keV can be modeled as a black body component with a temperature of $0.13_{-0.016}^{+0.011}$. An iron K_{α} line, with an EQW= 85.5_{-33}^{+27} , is also detected. The probability of the line being spurious is $\sim 10^{-14}$.

3C 227 is a Sy1 galaxy and also a Radio galaxy. The BAT spectrum is consistent with a power law model of photon index $1.96_{-0.58}^{+0.44}$. This source was detected at a level of 0.016 ct s^{-1} in a 11 ks long ROSAT-PSPC observation (0.1–2.4 keV) (Crawford & Fabian 1995). In order to match the ROSAT observed count rates, the extrapolation of the BAT power law to the 0.1–2.4 keV band requires an absorbing column density of at least 5×10^{21} atoms cm^{-2} . A recent Chandra observation confirms that 3C 227 is indeed an absorbed Sy1. However the joint Chandra-BAT spectrum is complex. Our best fit model is the sum of an absorbed power-law model and of a reflection component (both having the same photon index of $2.11_{-0.24}^{+0.14}$). The absorbing column density is $N_H=3.6_{-1.4}^{+1.5} \times 10^{22}$ atoms cm^{-2} . The reflection component seems to be large $R > 1$ which is at odds with the absence of the iron K_{α} line. This source certainly deserves further investigations.

NGC 3081 is mis-catalogged in SIMBAD as Sy1 galaxy. In fact the available 6dF spectrum shows clearly that this object is a Sy2 object. We have analyzed BeppoSax-MECS and ASCA data for this source. The best fit is a sum of a black body component, peaking at $0.58_{-0.11}^{+0.15}$ keV, an absorbed power law with column density of $60_{-3.1}^{+3.1} \times 10^{22}$ atoms cm^{-2} and photon index $1.9_{-0.04}^{+0.02}$ and an iron line of equivalent width of 241_{-131}^{+184} eV.

Table 1. Spectral parameters

NAME	RA (J2000)	DEC (J2000)	Type	$\Gamma/E[\text{kT}]^a$	N_H ($10^{22} \text{atoms cm}^{-2}$)	MODEL	INSTR. ^b
3C 105.0	61.9178	3.6517	Sy2	$1.66^{+0.13}_{-0.13}$	$29.4^{+5.7}_{-4.8}$	wabs*pow	B, X
1AXG J042556-5711	66.6021	-57.1775	Sy1	$1.54^{+0.028}_{-0.027}$	0	pow	B, A
3C 120	68.2982	5.3374	Sy1	$1.80^{+0.04}_{-0.04} / 0.27^{+0.026}_{-0.025}$	0	wabs*pow+bb	B, A
MCG -01-13-025	72.9205	-3.8240	Sy1.2	$1.6^{+0.48}_{-0.47}$	< 0.02 (1)	pow	B
SWIFT J0505.7-2348	76.4674	-23.8666	Sy2	$1.77^{+0.08}_{-0.07}$	$4.8^{+0.9}_{-0.7}$	wabs*pow	B, X
CSV 6150	77.7224	16.5265	Sy1.5	$1.94^{+0.25}_{-0.23}$...	pow	B
4U 0513-40	78.5146	-40.0558	LXB	$29.7^{+7.5}_{-5.8}$...	brem	B
QSO B0513-002	79.0096	-0.1332	Sy1	$1.83^{+0.02}_{-0.016} / 0.27^{+0.02}_{-0.02}$	< 0.01	wabs*pow+bb	B, A
SWIFT J0517.1+1633	79.2839	16.5605	...	$2.0^{+0.23}_{-0.26}$...	pow	B
ESO 362- G 018	79.8844	-32.6720	Sy1.5	$1.5^{+0.03}_{-0.02}$	<0.01	wabs*pow	B,X
Pictor A	79.9460	-45.7557	Sy1	$1.8^{+0.015}_{-0.014}$	$0.12^{+0.007}_{-0.02}$	wabs*pow	B, A
ESO 362-G021	80.6581	-36.4233	BL Lac	$1.7^{+0.037}_{-0.036}$	$0.1^{+0.0197}_{-0.0187}$	wabs*pow	B, A, X
V* TV Col	82.3541	-32.7965	CV-DQ*	$24.9^{+4.6}_{-3.8}$...	bremss	B
V* TW Pic	83.6470	-58.0200	CV	$13.5^{+10.6}_{-5.6}$...	bremss	B
LMC X-3	84.7717	-64.1148	HXB	$2.0^{+0.4}_{-0.3}$...	pow	B
LMC X-1	84.8917	-69.7210	HXB	$2.3^{+0.22}_{-0.20}$...	pow	B
PSR B0540-69.3	84.9878	-69.3230	Pulsar	$1.85^{+0.28}_{-0.26}$...	pow	B
PKS 0537-286	84.9953	-28.7029	BLAZAR	$1.35^{+0.06}_{-0.08}$	< 0.01	wabs*pow	B, A
PKS 0548-322	87.7165	-32.2610	BL Lac	$1.8^{+0.032}_{-0.031}$	$0.02^{+0.006}_{-0.005}$	wabs*pow	B, X
NGC 2110	88.0411	-7.4554	Sy2	$1.62^{+0.01}_{-0.01} / 0.47^{+0.02}_{-0.02}$	$4.0^{+0.13}_{-0.07}$	wabs*(pow+ga) + bb	B, A, X
LEDA 75476	89.5237	-38.3799	Sy1	$1.74^{+0.017}_{-0.025} / 0.25^{+0.08}_{-0.05}$	$2.5^{+0.11}_{-0.17}$	wabs*(pow+ga)+bb	B, A
ESO 490- G 26	100.0031	-25.8931	Sy1.2	$1.90^{+0.05}_{-0.04}$	$0.27^{+0.005}_{-0.005}$	wabs*pow	B, X
SWIFT J0727.5-2406	111.8951	-24.1039	...	$1.53^{+0.35}_{-0.54}$...	pow	B
V* 441 Pup	112.1626	-26.0696	CV	$12.4^{+13.6}_{-5.6}$...	bremss	B
V* BG CMi	112.8752	9.9214	CV	$31.3^{+41.2}_{-14.2}$...	bremss	B
SWIFT J0732.5-1331	113.1328	-13.5037	CV	$33.2^{+50.1}_{-14.2}$...	bremss	B
SWIFT J0739.6-3144	114.9127	-31.7496	Sy2 ^d	$1.77^{+0.51}_{-0.43}$	>2 ^c	pow	B
SWIFT J0743.0-2543	115.7501	-25.7314	...	$1.78^{+0.69}_{-0.56}$...	pow	B
IGR J07597-3842	119.9822	-38.7422	Sy1.2	$1.8^{+0.08}_{-0.07}$	<0.01	wabs*pow	B, X
UGC 4203	121.0552	5.1203	Sy2	$1.68^{+0.09}_{-0.10} / 0.31^{+0.08}_{-0.05}$	$12.5^{+5.0f}_{-3.7}$	wabs(pexrav+ga)+bb	B, A, X
SWIFT J0811.5+0937	122.8750	9.6214	XBONG ^d	$2.2^{+2.1}_{-0.9}$	0 ^e	pow	B
SWIFT J0823.4-0457	125.8271	-4.9401	Sy2	$1.84^{+0.28}_{-0.22}$	$19.3^{+6.8}_{-5.4}$	wabs*pow	B, X
Vela PSR	128.8308	-45.1771	PSR	$1.88^{+0.20}_{-0.26}$...	pow	B
FRL 1146	129.6151	-35.9976	Sy1	$1.88^{+0.37}_{-0.31}$...	pow	B

Table 1—Continued

NAME	RA (J2000)	DEC (J2000)	Type	$\Gamma/E[\text{kT}]^a$	N_H ($10^{22} \text{atoms cm}^{-2}$)	MODEL	INSTR. ^b
3C 206	129.9556	-12.2467	QSO	$1.95^{+0.43}_{-0.39}$	0^e	wabs*pow	B
SWFIT J0844.9-3531	131.2411	-35.5313	...	$1.91^{+0.46}_{-0.68}$...	pow	B
SWIFT J0854.7+1502	133.6828	15.0371	Sy2 ^d	$1.41^{+0.7}_{-0.9}$	$> 0.5^c$	pow	B
SWIFT J0917.2-6221	139.112	-62.359	Sy1	$1.87^{+0.07}_{-0.04} / 0.14^{+0.02}_{-0.02}$	$1.33^{+0.18}_{-0.10}$	bb+wabs*pow	B
Mrk 0704	139.6505	16.2987	Sy1.5	$1.36^{+0.1}_{-0.07}$	$15.0^{+6.3}_{-3.5}$	pcfabs*(pow+ga)	B, A, X
4U 0919-54	140.0753	-55.2135	LXB	$45.11^{+26.13}_{-9.8}$...	bremss	B
MCG -01-24-012	140.2134	-8.0872	Sy2	$1.7^{+0.08}_{-0.07}$	$6.5^{+0.8}_{-0.7}$	wabs*pow	B, X
NGC 2992	146.4060	-14.3007	Sy1.9	$1.24^{+0.06}_{-0.05}$	$0.17^{+0.03}_{-0.03}$	wabs*(pow+ga)	B, A, X
ESO 434- G 040	146.9151	-30.9388	Sy2	$1.77^{+0.006}_{-0.07} / 0.15^{+0.011}_{-0.016}$	$1.5^{+0.026}_{-0.09}$	wabs*(pow+ga)+bb	B, A, X
3C 227	146.9447	7.4191	Sy1	$2.11^{+0.14}_{-0.24}$	3.6	pextrav+wa*pow	B, C
NGC 3081	149.8805	-22.8561	Sy2	$1.9^{+0.02}_{-0.04} / 0.58^{+0.15}_{-0.11}$	$60^{+3.1}_{-3.1}$	wabs*(pow+ga) +bb	B, A, S

^aPhoton index and/or plasma temperature for the model, specified in column “Model”, to fit the data.

^bInstrument used for spectral analysis are: B = BAT, X = Swift/XRT, A = ASCA, C = Chandra, and S = BeppoSAX.

^c Lower limit on absorption estimated through the non detection by ROSAT

^dProposed identification in Rau et al. (2007).

^eOrder of magnitude of the absorption estimated imposing that the extrapolated source flux match the ROSAT-PSPC count rates.

^fUGC 4203 exhibits transition between reflection-dominated and a transmission-dominated spectrum. The absorption is estimated in the latter case using XRT data (see text for details).

References. — References: (1) Gallo et al. (2005).

Table 2. Spectral parameters for Sy1, Sy2, intermediate and all Seyfert AGN. Errors are 90% confidence level.

CLASS	Photon index	χ^2 /NDF
Seyfert 1	2.23 ± 0.11	5.4/4
Seyfert 2	1.86 ± 0.10	1.2/4
Seyfert 1.2-1.5	1.95 ± 0.11	4.9/4
Seyfert All	2.00 ± 0.07	2.1/4

Table 3. Extragalactic sample.

NAME	Type	z	Radio-loudness	F _x (10 ⁻¹¹ erg cm ⁻² s ⁻¹)	L _x (10 ⁴³ erg s ⁻¹)	L _{2-10 keV} /L _{OIII} ^a	Fe _{EW} ^b (eV)	N _H (10 ²² atoms cm ⁻²)	ref
3C 105.0	Sy2	0.089	28421	4.6 ^{+0.5} _{-0.4}	44.5 ⁺¹⁷ ₋₂₂	581.5±69.2	nr	29.4	1
1AXG J042556-5711	Sy1	0.104	0.78 ^c	1.92 ^{+0.2} _{-0.2}	55.0 ⁺¹⁰ ₋₈	...	nr	0	1
3C 120	Sy1	0.0330	3762	10.1 ^{+0.8} _{-1.8}	25.4 ^{+2.2} _{+4.5}	148.8±40.6	52.3	0	1
MCG -01-13-025	Sy1.2	0.015894	1.15 ^c	2.52 ^{+1.1} _{-1.6}	1.5 ^{+0.6} _{-0.8}	<0.02	2
SWIFT J0505.7-2348	Sy2	0.0350	7.13 ^c	5.0 ^{+0.7} _{-1.5}	14.1 ^{+0.24} _{-5.0}	345.2±82.2	nr	6.3	1
QSO B0513-002	Sy1	0.0327	0.254	4.92 ^{+0.9} _{-2.8}	12.3 ^{+2.1} _{-7.3}	...	90.8	0.02	3
ESO 362- G 018	Sy1.5	0.0126	0.58 ^c	5.0 ^{+0.7} _{-1.0}	1.7 ^{+0.3} _{-0.3}	36.3±3.7	nr	<0.01	1
Pictor A	Sy1	0.035	14045	1.8 ^{+0.4} _{-1.2}	5.1 ^{+1.5} _{-3.7}	113.4±14.5	nr	0.12	1
ESO 362-G021	BL Lac	0.05534	2409	2.7 ^{+0.3} _{-0.3}	18.8 ^{+5.0} _{-0.5}	1284.1±270.3	nr	0.1	1
PKS 0537-286	BLAZAR	3.1	22000	2.43 ^{+0.9} _{-3.0}	1.2 ^{+0.4} × 10 ⁵	...	nr	<0.01	1
PKS 0548-322	BL Lac	0.0690	383.33	3.1 ^{+0.6} _{-1.0}	37.0 ^{+6.0} _{-11.0}	...	nr	0.0257	1
NGC 2110	Sy2	0.007789	26.92	27.0 ^{+0.9} _{-1.0}	3.5 ^{+0.1} _{-0.1}	1115.8±101.4	118	4.0	1
LEDA 75476	Sy1	0.0338	2.87 ^c	3.2 ^{+0.6} _{-1.2}	8.7 ^{+2.4} _{-2.1}	393.7±59.6	144	2.5	1
UGC 4203	Sy2	0.01349	7.67	4.28 ^{+0.6} _{-1.4}	1.7 ^{+0.3} _{-0.6}	214.2±71.4	747	12.5	1
SWIFT J0811.5+0937	XBONG	0.282	268 ^c	1.55 ^{+1.2} _{-1.54}	384 ⁺¹⁷⁰ ₋₂₀₀	~ 0 ^d	1
SWIFT J0823.4-0457	Sy2	0.023	0.61 ^c	2.78 ^{+1.0} _{-1.1}	3.3 ^{+1.1} _{-1.3}	179.1±71.6	...	16.2	1
3C 206	QSO	0.1976	1194	2.62 ^{+0.7} _{-1.3}	300 ⁺⁷⁵ ₋₁₁₆	0	1
SWIFT J0854.7+1502	Sy2	0.0696	...	1.73 ^{+1.3} _{-1.5}	19.7 ⁺¹³ ₋₁₆	> 0.5 ^d	1
Mrk 0704	Sy1	0.0292	0.82 ^c	2.21 ^{+1.1} _{-0.9}	4.3 ^{+2.1} _{-1.8}	114.9±27.1	160	14.6	1
MCG -01-24-012	Sy2	0.01964	2.86 ^c	4.6 ^{+0.7} _{-0.9}	3.7 ^{+0.4} _{-0.6}	2914.4±1092.9	nr	6.8	1
NGC 2992	Sy1.9	0.00771	2.03	3.6 ^{+1.0} _{-1.1}	0.47 ^{+0.13} _{-0.10}	0.8±0.1	520	0.17	1
ESO 434- G 040	Sy2	0.00848	0.6	19.1 ^{+0.6} _{-0.6}	2.7 ^{+0.1} _{-0.1}	912.9±21.1	85.5	1.5	1
3C 227	Sy1	0.0858	5462	2.23 ^{+0.3} _{-1.6}	40.0 ^{+1.0} _{-3.2}	19.3±7.10	nr	3.6	1
NGC 3081	Sy2	0.00798	0.1 ^c	6.8 ^{+0.9} _{-0.8}	0.96 ^{+0.1} _{-0.11}	31.0±1.7	241	60	1

^aThe OIII luminosities have been derived in Rau et al. (2007).

^bIron line equivalent width. A value of “nr” means that the iron line is statistically not required by the fit.

^cThe radio flux at other wavelengths has been extrapolated to 6 cm assuming $f_\nu \propto \nu^{-0.5}$.

^d Limit on the absorption obtained extrapolating the BAT spectrum to the ROSAT band.

References. — References for the absorption values: (1) this work; (2) Gallo et al. (2005); (3) Lutz et al. (2004).

Table 4. Comparison with previous results

Instrument	Ref.	Energy keV	AGN density ^a 10^{-2} deg^{-2}	BAT density (this work) ^b 10^{-2} deg^{-2}
INTEGRAL-ISGRI	1	20 - 40	0.48 ± 0.08	0.41 ± 0.08
INTEGRAL-ISGRI	2	100 - 150	0.18 ± 0.006	0.17 ± 0.034
HEAO-1 A2	3	2 - 10	1.2 ± 0.2	1.6 ± 0.32
RXTE PCA	4	8 - 20	0.56 ± 0.06	0.65 ± 0.13
XMM	5	0.5 - 2	0.1 ± 0.01	1.3 ± 0.26
XMM	5	2 - 10	0.95 ± 0.06	1.6 ± 0.32
XMM	5	5 - 10	0.63 ± 0.4	0.4 ± 0.08

^aAGN densities from different surveys above $10^{-11} \text{ erg cm}^{-2} \text{ s}^{-1}$ (in the respective bands).

^bThe BAT AGN density was converted to the native energy band of the measurement we are comparing it with.

References. — (1) Beckmann et al. 2006; (2) Bazzano et al. 2006; (3) Piccinotti et al. 1982; (4) Revnivtsev et al. 2004; (5) Cappelluti et al. 2007

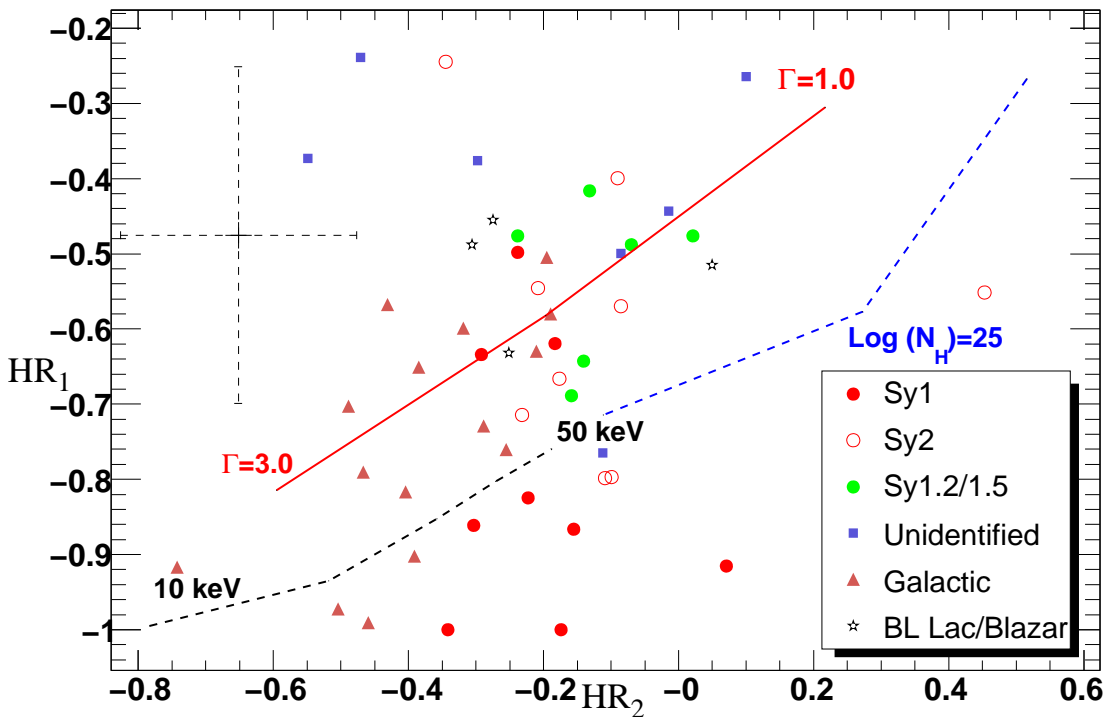


Fig. 1.— Plot of HR1 and HR2 hardness ratios. The solid line is the locus for sources with unabsorbed power law spectra with photon indices from 1.0 to 3.0 while the long dashed line shows the location of Compton-thick AGN with the same range of photon indices. The dashed line shows the location of objects with a thermal bremsstrahlung spectrum with temperatures in the range 5–50 keV. In the upper left corner the typical $\pm 1\sigma$ error for a 5σ source is shown.

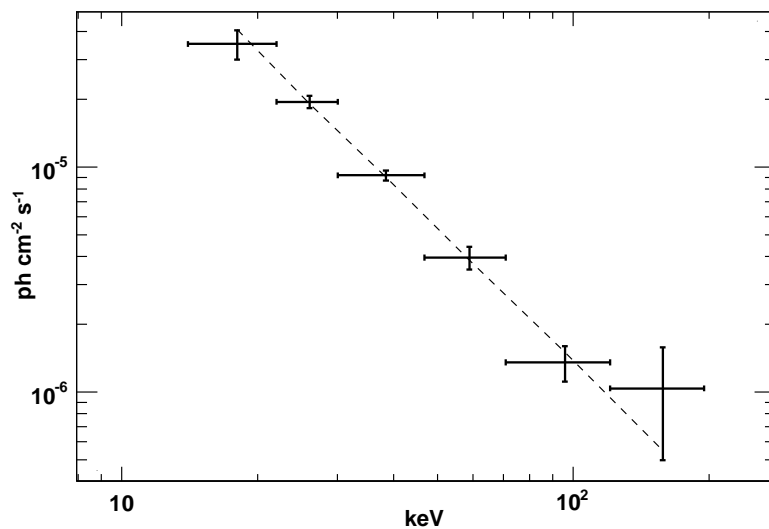


Fig. 2.— Stacked spectrum of all AGN reported in Tab. 3 excluding the Blazars. The dashed line is the best power-law fit to the data (photon index 2.0 ± 0.07 .)

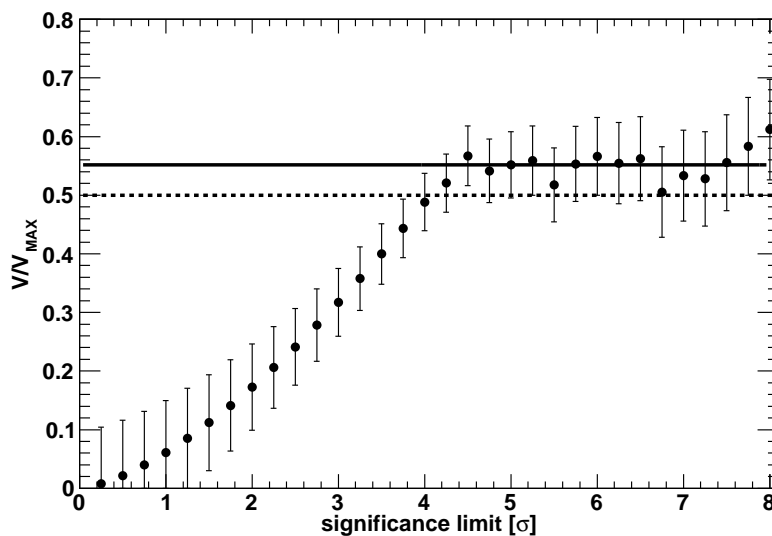


Fig. 3.— V/V_{MAX} as a function of detection threshold for the sample of extragalactic sources. The dashed line is the expected value (0.5) for a complete sample in an homogeneous distribution. The solid line shows the mean test value for $S/N > 4.5\sigma$.

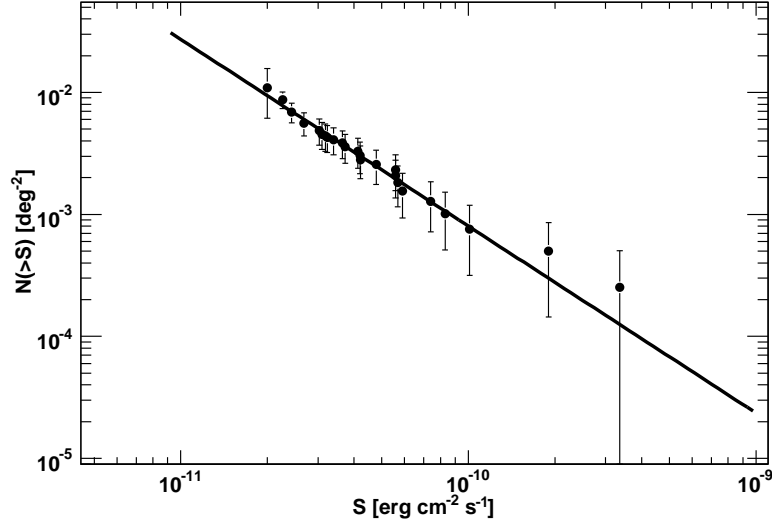


Fig. 4.— Extragalactic cumulative source count distribution in the 14-170 keV band. The solid line is the best fit described in the text.

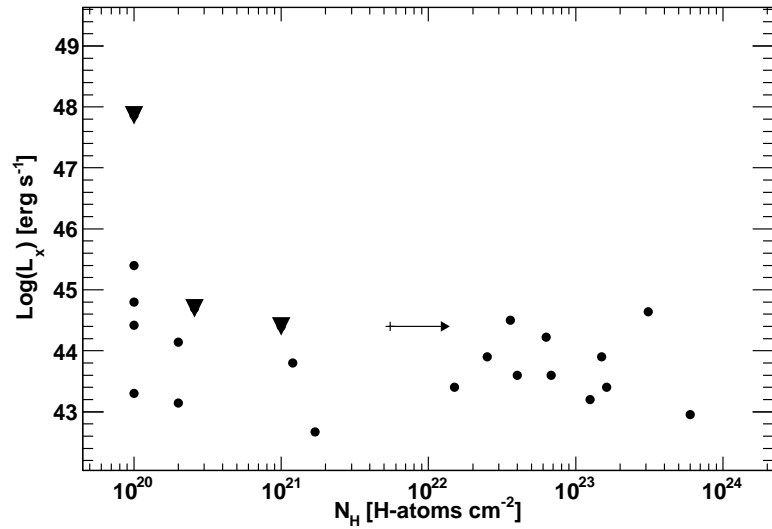


Fig. 5.— Luminosity, in the 14-170 keV band, vs. intrinsic column density for the extragalactic sample. The blazars are highlighted with a triangle.

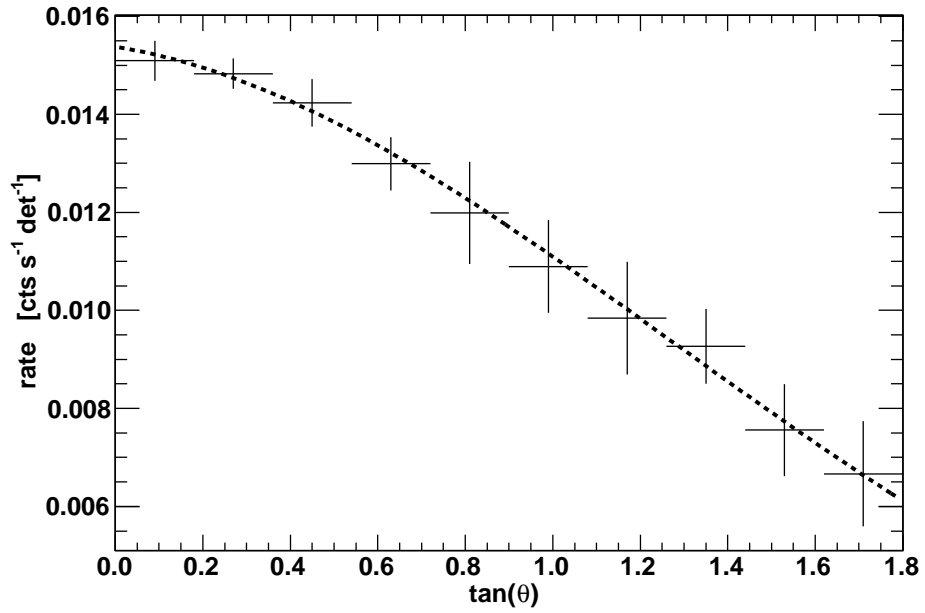


Fig. 6.— Crab rates in the 14-22 keV band as a function of the tangent of the off-axis angle. When the Crab is 50° off-axis the detected count rate is ~30% lower than the on-axis count rate. The solid line is a polynomial fit to the rates.

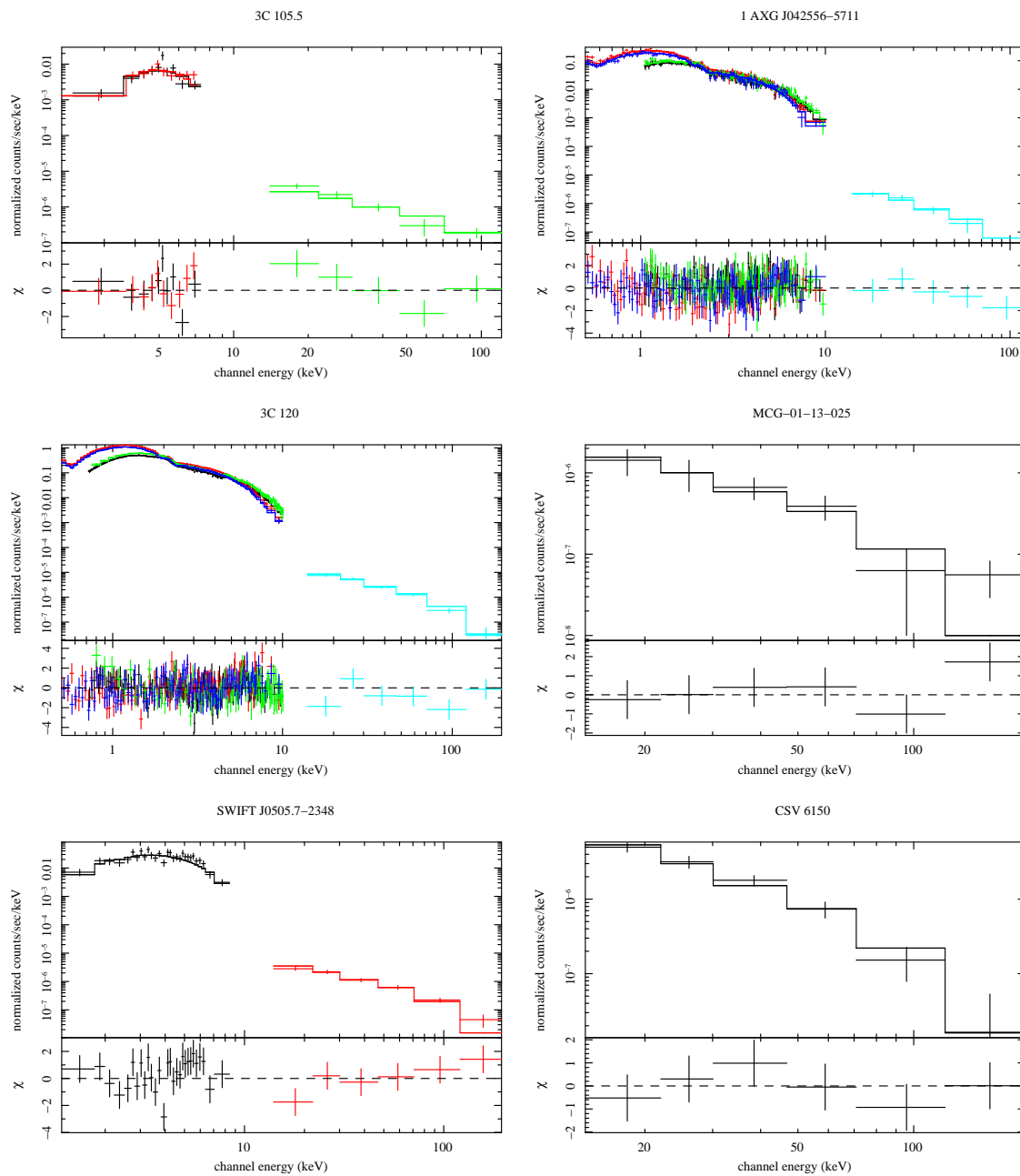


Fig. 7.— Folded spectra and best fit models as described in the text. From left to right and up to bottom the spectra are for: 3C105.0, 1AXG J042556-5711, 3C120, MCG-01-13-025, SWIFT J0505.7-2348 and CSV6150.

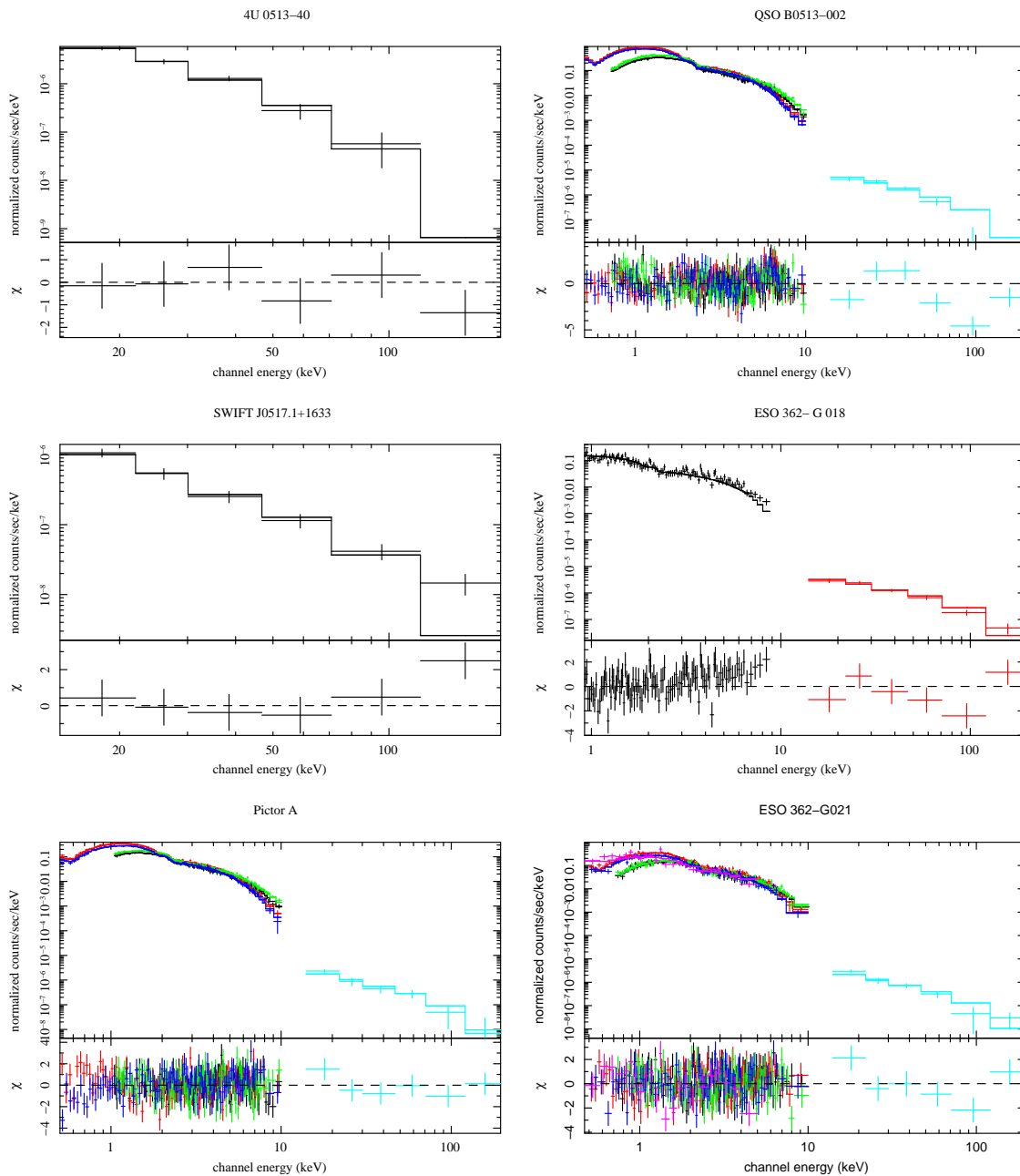


Fig. 8.— (for online version) Folded spectra and best fit models as described in the text. From left to right and up to bottom the spectra are for: 4U 0513-40, QSO B0513-002, SWIFT J0517.1+1633, ESO 362- G 018, Pictor A and ESO 362- G 021.

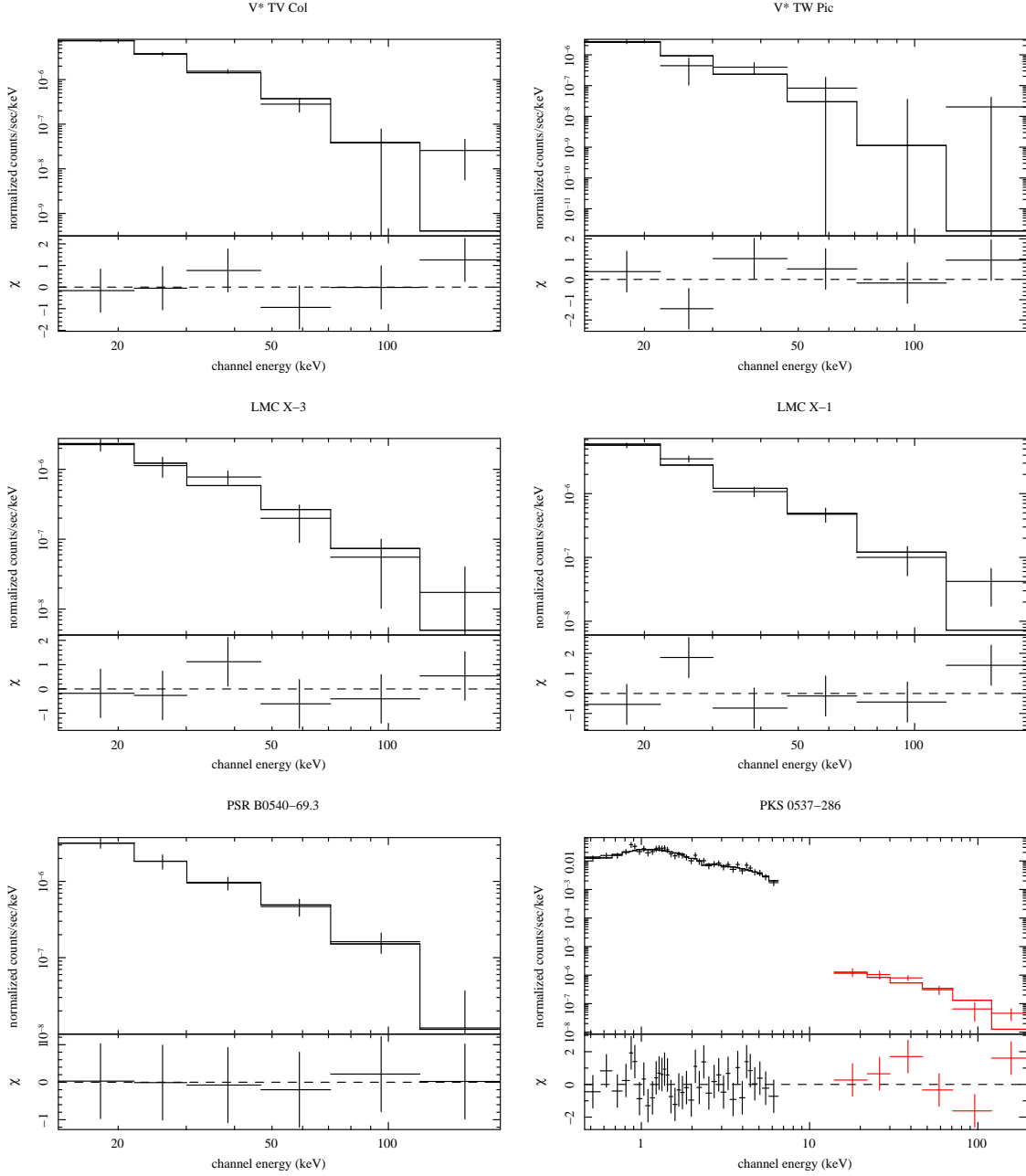


Fig. 9.— (for online version) Folded spectra and best fit models as described in the text. From left to right and up to bottom the spectra are for: TV Col, TW Pic, LMC X-3, LMC X-1, PSR B0540-69.3 and PKS 0537-286.

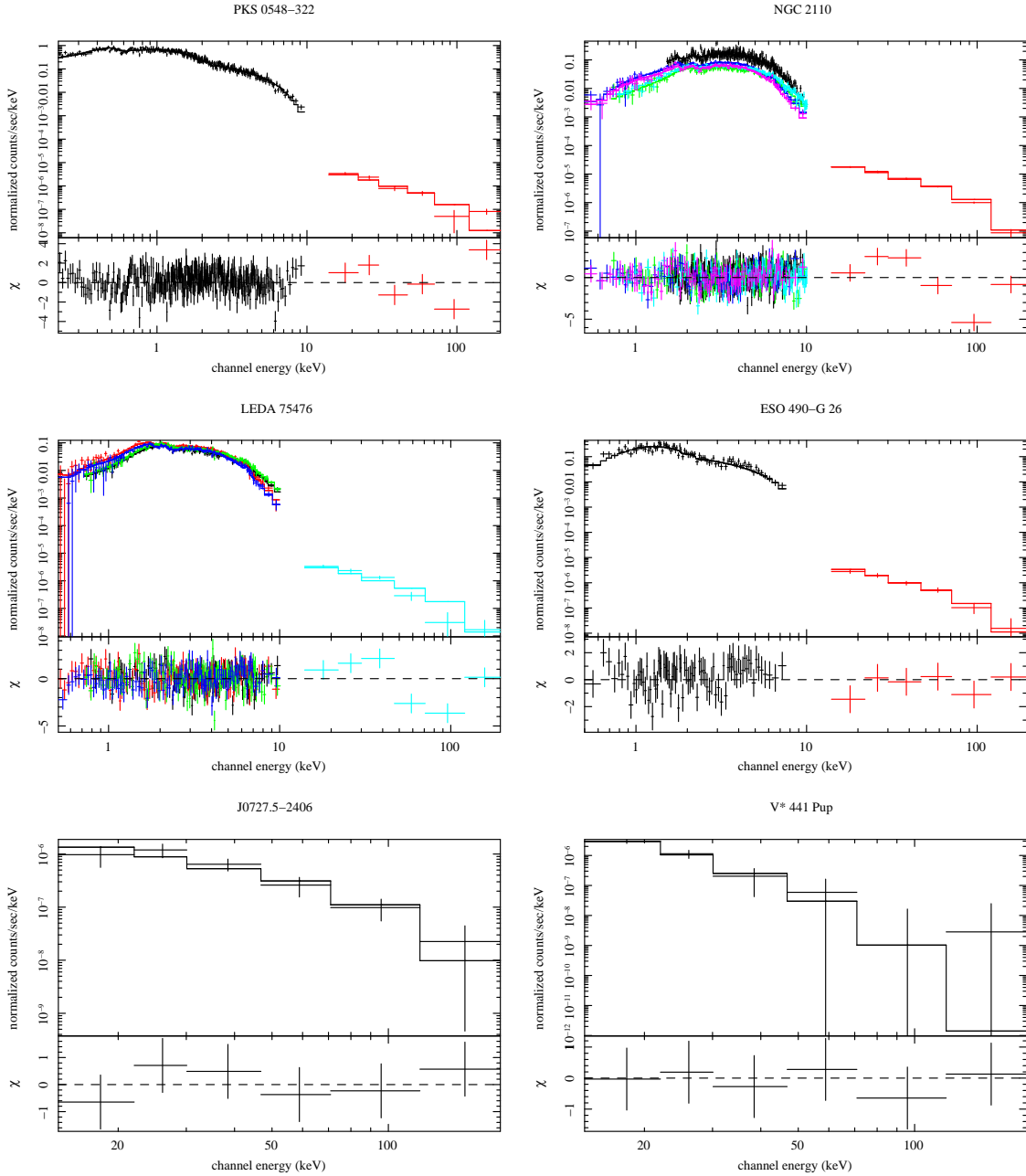


Fig. 10.— (for online version) Folded spectra and best fit models as described in the text. From left to right and up to bottom the spectra are for: PKS 0548-322, NGC 2110, LEDA 75476, ESO 490- G 26, J0727.5-2406 and V441 Pup

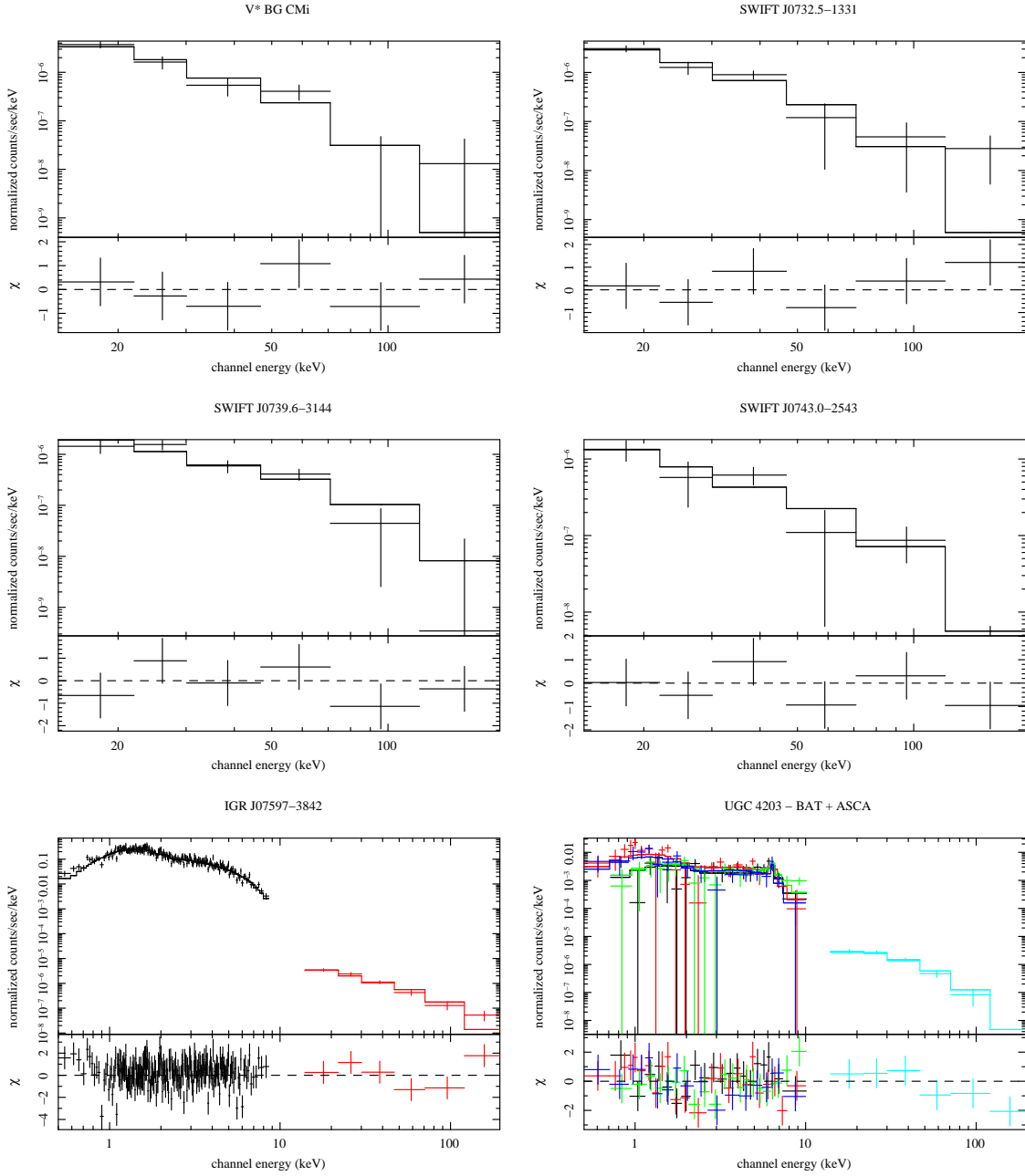


Fig. 11.— (for online version) Folded spectra and best fit models as described in the text. From left to right and up to bottom the spectra are for: BG CMi, J0732.5-1331, J0739.6-3144, J0743.0-2543, IGR K07597-3842 and UGC 4203.

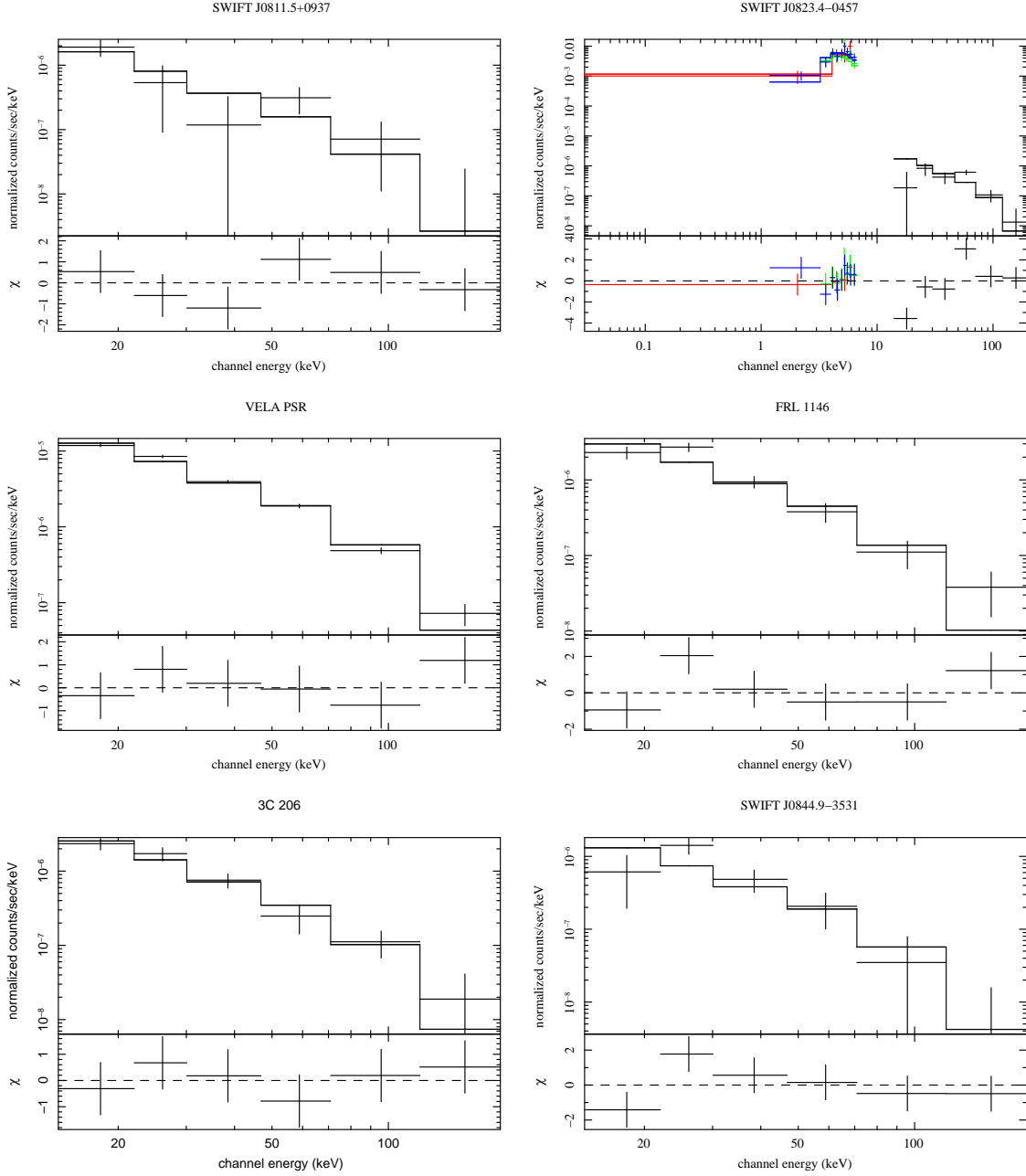


Fig. 12.— (for online version) Folded spectra and best fit models as described in the text. From left to right and up to bottom the spectra are for: J0811.5+0937, J0823.4-0457, VELA PSR, FRL 1146, 3C 206 and J0844.9-3531.

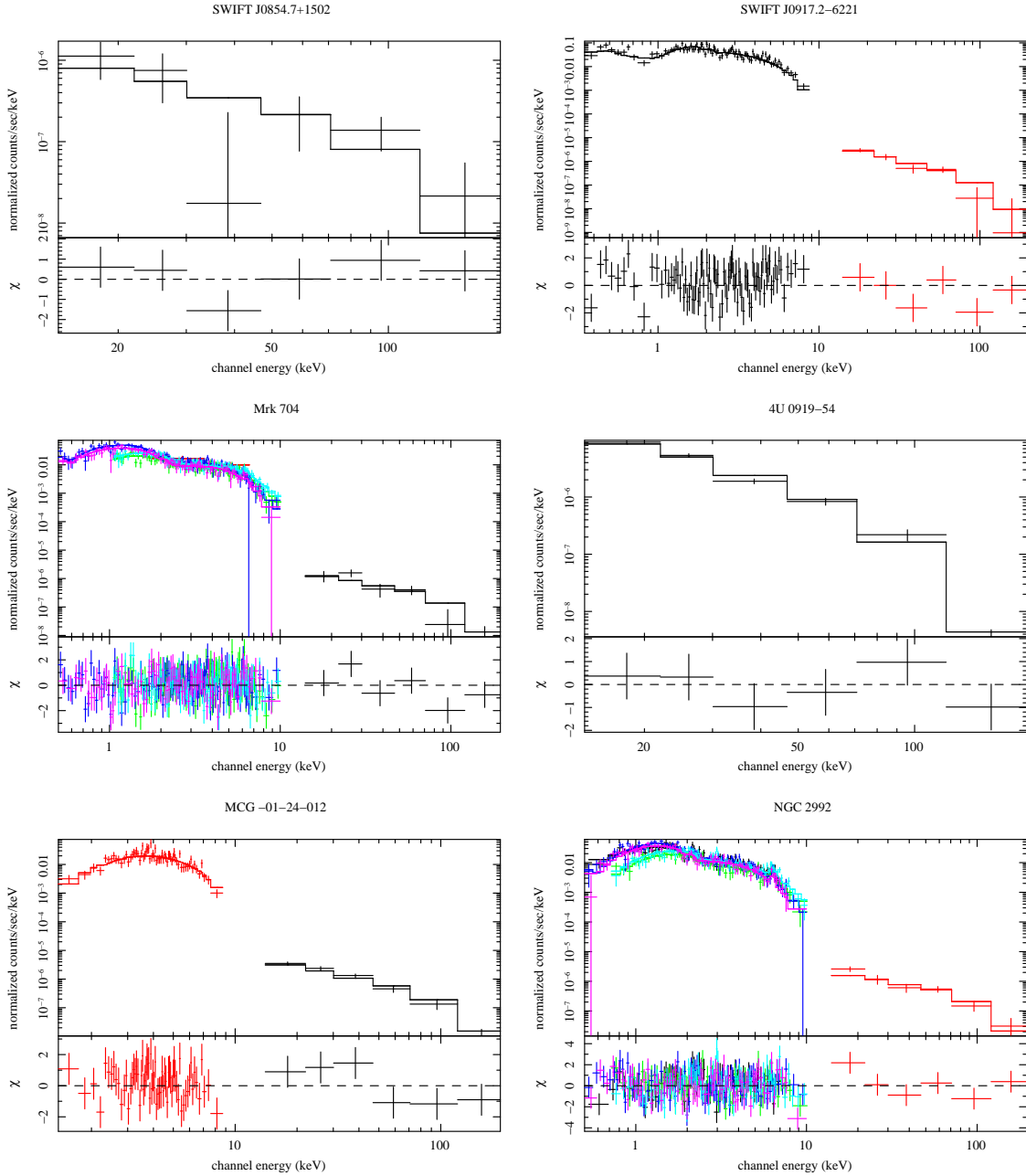


Fig. 13.— (for online version) Folded spectra and best fit models as described in the text. From left to right and up to bottom the spectra are for: J0854.7+1502, J0917.2-6221, Mrk 704, 4U 0919-54, MCG -01-24-012 and NGC 2992.

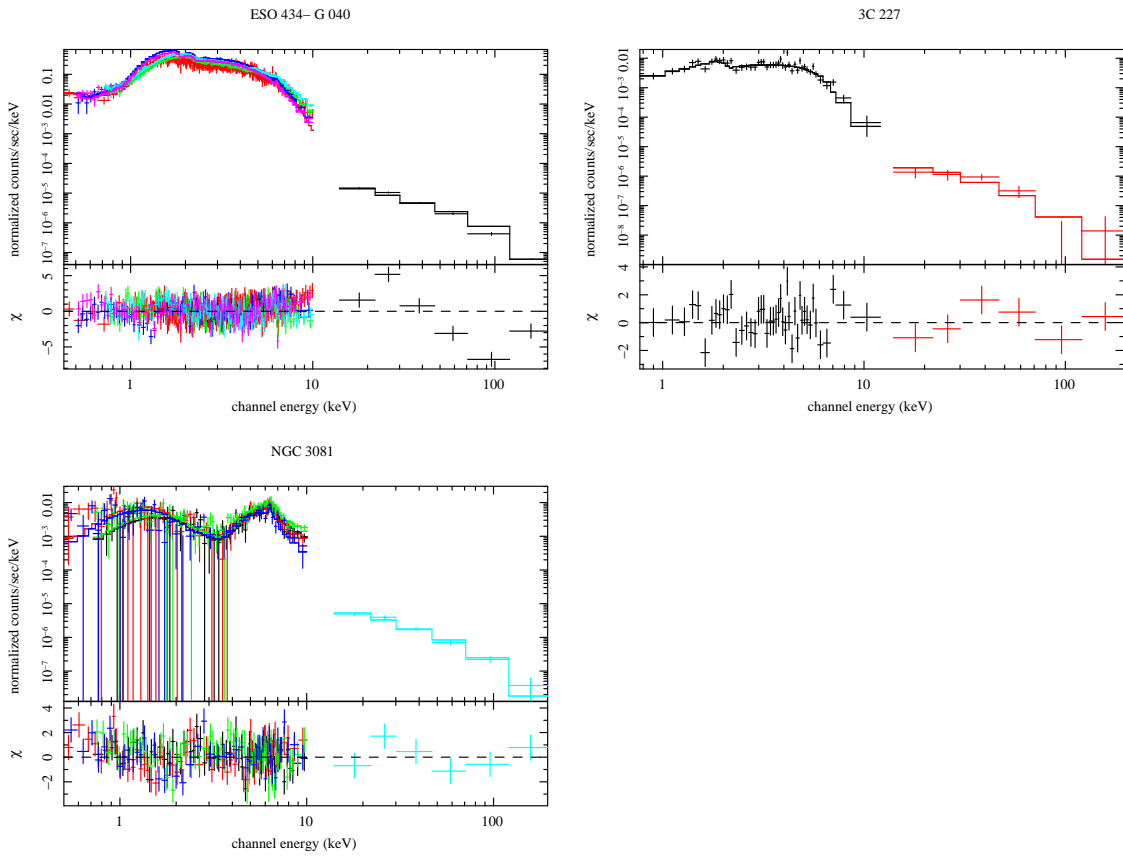


Fig. 14.— (for online version) Folded spectra and best fit models as described in the text. From left to right and up to bottom the spectra are for: ESO 434 -G 040, 3C 227 and NGC 3081.